ELSEVIER

Coordination Chemistry Reviews 229 (2002) 75–93

COORDINATION CHEMISTRY REVIEWS

www.elsevier.com/locate/ccr

Energy transfer and harvesting in $[Ru_{1-x}Os_x(bpy)_3](PF_6)_2$ and $\{\Lambda\text{-}[Ru(bpy)_3]\Delta\text{-}[Os(bpy)_3]\}(PF_6)_4$

Hartmut Yersin [1,*], Cornelius Kratzer

Institut für Physikalische und Theoretische Chemie, Universität Regensburg, D-93040 Regensburg, Germany

Received 7 December 2001; accepted 28 March 2002

Contents

* Corresponding author. Tel.: +49-941-943-4464; fax: +49-941-943-4488
E-mail address: hartmut.yersin@chemie.uni-regensburg.de (H. Yersin).
[1] Homepage: http://www.uni.regensburg.de/ ~ hartmut.yersin

0010-8545/02/$ - see front matter
PII: S0010-8545(02)00106-6

Abstract

{Λ-[Ru(bpy)$_3$]Δ-[Os(bpy)$_3$]}(PF$_6$)$_4$ is the first representative of a new class of materials. The crystal structure is built up of homochiral layers of Λ-[Ru(bpy)$_3$]$^{2+}$ that alternate with homochiral layers of Δ-[Os(bpy)$_3$]$^{2+}$. In this new material, the excitation energy is transferred efficiently by radiationless processes to one single crystallographic site of Δ-[Os(bpy)$_3$]$^{2+}$ (site A), where the excitation energy is harvested. We develop an understanding of: (1) the different steps of energy transfer, (2) the dominating mechanisms (Förster and/or Dexter), and (3) the electronic states involved. Therefore, we study, typically at $T = 1.3$ K, properties of the low-lying excited states and of energy transfer processes occurring in rac-[Ru(bpy)$_3$](PF$_6$)$_2$, [Ru$_{1-x}$Os$_x$(bpy)$_3$](PF$_6$)$_2$ (with $x =$ 0.01, 0.1, 0.2, and 1.0) and we compare the results to those obtained for {Λ-[Ru(bpy)$_3$]Δ-[Os(bpy)$_3$]}(PF$_6$)$_4$. It can be concluded for this latter compound that the different inter-layer and intra-layer steps of energy transfer to the lowest site of Δ-[Os(bpy)$_3$]$^{2+}$ are dominated by efficient Dexter exchange processes. Due to energy accumulation at this lowest site, the new compound exhibits the interesting property of self-site-selectivity. This means, one obtains one-site emission spectra for every excitation wavelength from the UV to 693 nm. And since this lowest site of Δ-[Os(bpy)$_3$]$^{2+}$ is well shielded from its environment, the spectra are highly resolved and thus reveal directly detailed properties of the low-lying electronic states and their vibronic coupling behavior. In particular, these properties depend strongly on an applied magnetic field. For example, with application of a field up to $H = 12$ T, the intensity of the lowest electronic 0–0 transition can be tuned in and increased by several orders of magnitude. Simultaneously, the vibrational satellite structure is completely altered. We observe changes from a vibronically induced (Herzberg–Teller) structure to a structure dominated by Franck–Condon satellites. This property of Δ-[Os(bpy)$_3$]$^{2+}$ is due to a magnetically induced coupling between lower lying triplet substates. Similar observations have not yet been reported for other compounds.

Keywords: Radiationless energy transfer; Energy harvesting; Self-site-selectivity; Magnetic field effects; Hetero-chirality; [Ru(bpy)$_3$]$^{2+}$; [Os(bpy)$_3$]$^{2+}$

1. Introduction

Properties of the lowest excited and emitting triplet states and of the singlet ground states of [Ru(bpy)$_3$]$^{2+}$ and [Os(bpy)$_3$]$^{2+}$ are in the focus of many research groups since more than three decades. This is due to a number of potential applications (e.g. see [1–4]) as well as due to important scientific questions, such as effects of localization/delocalization in the lowest excited states, the understanding of metal-to-ligand charge transfer (MLCT) transitions, vibronic coupling properties, spin-lattice relaxations (SLR), etc. (e.g. see [5] and the references therein). In particular, in spatially adjacent or coupled [Ru(bpy)$_3$]$^{2+}$–[Os(bpy)$_3$]$^{2+}$ or related systems one usually finds radiationless energy transfer from the energetically higher lying donor states of [Ru(bpy)$_3$]$^{2+}$ to the lower lying acceptor states of [Os(bpy)$_3$]$^{2+}$. These processes have first been studied already 15 years ago in crystalline [Ru(bpy)$_3$](PF$_6$)$_2$ doped with small amounts of [Os(bpy)$_3$]$^{2+}$ by Yersin and co-workers [6–8] and in covalently linked dinuclear compounds by Furue et al. [9]. Subsequently, many interesting new systems were created, in which mostly Ru(II)– and Os(II)–2,2′-bipyridine fragments are connected by various kinds of bridges that are different with respect to donor–acceptor separations, electronic coupling properties and steric confinements (e.g. see [10–20]). It is further referred to more recent investigations of energy transfer between Ru(II)– and Os(II)–polypyridine complexes in crystalline materials [21–24] and in Langmuir–Blodgett films [25]. In the present contribution, we follow a different approach and study the energy transfer in the newly engineered neat crystalline material {Λ-[Ru(bpy)$_3$]-Δ-[Os(bpy)$_3$]}(PF$_6$)$_4$. This heteroracemic compound consists of alternating layers of Λ-[Ru(bpy)$_3$]$^{2+}$ and Δ-[Os(bpy)$_3$]$^{2+}$ [26,27]. Interestingly, at low temperature one crystallographic site (site A) of the [Os(bpy)$_3$]$^{2+}$ acceptors has a slightly lower energy. As a consequence, the excitation energy is harvested at this site and only this site emits. Moreover, this specific site is electronically well shielded (no neighbors with resonant energies) and is characterized by its well-defined environment (small inhomogeneities). Thus, highly resolved emission spectra of just one site can easily be monitored irrespectively of the excitation wavelength. This unusual behavior can be used to develop a better understanding of the electronic structure of the lower excited states of [Os(bpy)$_3$]$^{2+}$.

The present paper is organized as follows: After a short presentation of crystal structures and a discussion of differences of nearest neighbor arrangements which are important for energy transfer pathways in Section 2, electronic states, emission properties and processes of energy transfer occurring in neat racemic [Ru(bpy)$_3$](PF$_6$)$_2$ are discussed in Section 3. In Section 4, we treat properties of this neat rac-[Ru(bpy)$_3$](PF$_6$)$_2$ material doped with Δ-[Os(bpy)$_3$]$^{2+}$ including neat rac-[Os(bpy)$_3$](PF$_6$)$_2$. Section 5 presents the specific effects of a directed radiationless energy transfer observed in {Λ-[Ru(bpy)$_3$]Δ-[Os(bpy)$_3$]}(PF$_6$)$_4$. Further, photophysical properties of Δ-[Os(bpy)$_3$]$^{2+}$ are discussed in some detail by use of this new hetero-racemic compound and it is shown that emission properties are tunable by

application of high magnetic fields. Section 6 summarizes and concludes this contribution.

2. Structures

The structures discussed in this contribution undergo phase transitions below about 190 K. The room temperature (r.t.) phases, called β-phases, are characterized by high symmetry space groups and two complexes per unit cell, while the low-temperature structures (α-phases) have symmetry-reduced space groups and contain six complexes per unit cell. In the context of this investigation, we are mainly interested in the low-temperature α-phases.

2.1. Structure of rac-[Ru(bpy)$_3$](PF$_6$)$_2$

The r.t. structure of rac-[Ru(bpy)$_3$](PF$_6$)$_2$ (β-phase, space group $P3c1$) [28] undergoes a phase transition upon cooling. The resulting low-temperature structure (α-phase) has been determined by Bürgi and Ludi et al. [29] at $T = 105$ K. Fig. 1 shows a schematic diagram. The space group of this α-phase is $P31c$ and the unit cell with the lattice constants of $a = 18.338$ Å and $c = 16.216$ Å contains three Λ-[Ru(bpy)$_3$]$^{2+}$ and three Δ-[Ru(bpy)$_3$]$^{2+}$ isomers. It is characteristic of this structure that a close packed homochiral layer is arranged perpendicularly to the c-axis at $z \approx 1/4$ and that a second layer of opposite chirality is located at $z \approx 3/4$. Further, [Ru(bpy)$_3$]$^{2+}$ complexes of alternating chirality form columns along the c-axis with 3-fold axes. Three of such columns belong to one unit cell. A glide mirror plane containing the c-axis passes through one specific column at ($00z$) and thus relates, by symmetry, two cations of opposite chirality within just this same column. On the other hand, this glide mirror plane projects the [Ru(bpy)$_3$]$^{2+}$ complexes of one of the other two columns into the respective neighboring column.

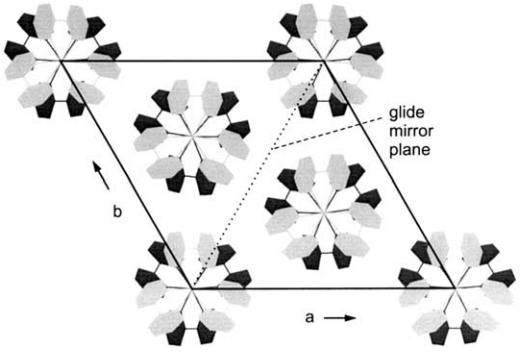

Fig. 1. Schematic structure of rac-[Ru(bpy)$_3$](PF$_6$)$_2$ at low temperature (α-phase). For clarity, the (PF$_6$)$^-$ cations are omitted. The c-axis and the glide mirror plane are perpendicular to the drawing plane. (Compare Ref. [29]).

In summary, the six [Ru(bpy)$_3$]$^{2+}$ complexes of the unit cell are grouped into sets of three independent crystallographic sites all exhibiting C_3 symmetry. The glide mirror plane relates in each case two complexes of opposite chirality. Those two specific complexes that lie in the same column and that are symmetry-related to each other are physically distinct.

2.2. Structure of {Λ-[Ru(bpy)$_3$]Δ-[Os(bpy)$_3$]}(PF$_6$)$_4$

It has been shown that the high temperature β-phase of rac-[Os(bpy)$_3$](PF$_6$)$_2$ is isomorphous [30,31] with the β-phase of rac-[Ru(bpy)$_3$](PF$_6$)$_2$. Thus, when rac-[Ru(bpy)$_3$](PF$_6$)$_2$ is doped with racemic [Os(bpy)$_3$]$^{2+}$ both Λ- and Δ-[Ru(bpy)$_3$]$^{2+}$ complexes can be replaced by the respective Λ- and Δ-[Os(bpy)$_3$]$^{2+}$ isomers. On the other hand, when only Δ-[Os(bpy)$_3$]$^{2+}$ is present as doping material—and when chiral recognition is an effective mechanism in the course of crystal growing—the Δ-[Os(bpy)$_3$]$^{2+}$ complexes should only be incorporated at Δ-sites of the packing of rac-[Ru(bpy)$_3$](PF$_6$)$_2$. Thus, Δ-[Os(bpy)$_3$]$^{2+}$ should be built in only in every second layer. Moreover, in heteroracemic 1:1 mixtures of Λ-[Ru(bpy)$_3$](PF$_6$)$_2$ and Δ-[Os(bpy)$_3$](PF$_6$)$_2$ (or vice versa) the homochiral Λ- and Δ-layers should consist of different cations. Due to the very similar sizes and shapes of [Ru(bpy)$_3$]$^{2+}$ and [Os(bpy)$_3$]$^{2+}$ it is expected that the topology of the packing is preserved. Indeed, as has been shown recently [26,27], this new type of crystal structure is really found.

The high-temperature β-phase of this engineered {Λ-[Ru(bpy)$_3$]Δ-[Os(bpy)$_3$]}(PF$_6$)$_4$ salt crystallizes in the space group $P321$ and the unit cell contains one Λ-[Ru(bpy)$_3$]$^{2+}$ and one Δ-[Os(bpy)$_3$]$^{2+}$ complex. In analogy to the situation described for neat rac-[Ru(bpy)$_3$](PF$_6$)$_2$, for the new compound one also observes a phase transition upon cooling to $T = 105$ K [26]. The

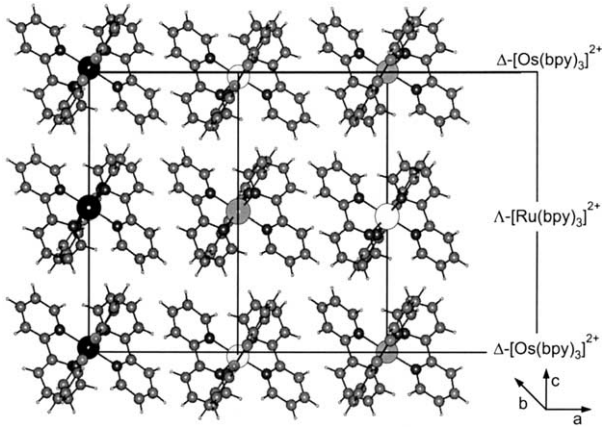

Fig. 2. Crystal packing diagram of {Λ-[Ru(bpy)$_3$] Δ-[Os(bpy)$_3$]}(PF$_6$)$_4$ ($T = 105$ K). The (PF$_6$)$^-$ anions are omitted. Note the slightly different z-coordinates of the cations within a single layer. (Compare Ref. [26]).

resulting α-phase of {Λ-[Ru(bpy)$_3$]Δ-[Os(bpy)$_3$]}(PF$_6$)$_4$ is characterized by the symmetry reduced space group $P3$ and by unit cell parameters of $a = 18.419$ Å and $c = 16.231$ Å. The unit cell contains three Λ-[Ru(bpy)$_3$]$^{2+}$ and three Δ-[Os(bpy)$_3$]$^{2+}$ complexes (= crystallographic sites) [26].

In summary, utilization of chirality allows for a controlled reduction of the space group symmetry resulting in a crystal that is built up from alternating [Ru(bpy)$_3$]$^{2+}$ and [Os(bpy)$_3$]$^{2+}$ layers (Fig. 2). As a consequence of this structure, close [Ru(bpy)$_3$]$^{2+}$–[Ru(bpy)$_3$]$^{2+}$ or [Os(bpy)$_3$]$^{2+}$–[Os(bpy)$_3$]$^{2+}$ contacts exist only in planes perpendicular to the columns (*ab*-planes), but the important contacts between equivalent chromophores along the columns are lost. Now Λ-[Ru(bpy)$_3$]$^{2+}$ and Δ-[Os(bpy)$_3$]$^{2+}$ alternate rigorously. Obviously, these different cations are no longer connected via glide mirror planes. These mirror planes are lost in this new hetero-racemic structure. Thus, three distinct crystallographic sites exist for Λ-[Ru(bpy)$_3$]$^{2+}$ and also for Δ-[Os(bpy)$_3$]$^{2+}$ [26].

2.3. Structures and various pathways of radiationless energy transfer

The various structures presented, provide distinct and well defined differences of energy transfer pathways due to different nearest neighbor situations. In particular, one finds symmetry-related and thus equivalent Λ- and Δ-isomers as nearest neighbors in the same column as well as in different columns in rac-[Ru(bpy)$_3$](PF$_6$)$_2$ and in rac-[Os(bpy)$_3$](PF$_6$)$_2$, respectively. On the other hand, in {Λ-[Ru(bpy)$_3$]Δ-[Os(bpy)$_3$]}(PF$_6$)$_4$, Λ-[Ru(bpy)$_3$]$^{2+}$ donors lie in one plane, while Δ-[Os(bpy)$_3$]$^{2+}$ acceptors are found in the neighboring planes. This structure provides also Λ-[Ru(bpy)$_3$]$^{2+}$–Λ-[Ru(bpy)$_3$]$^{2+}$ and Δ-[Os(bpy)$_3$]$^{2+}$–Δ-[Os(bpy)$_3$]$^{2+}$ in-plane as well as Λ-[Ru(bpy)$_3$]$^{2+}$–Δ-[Os(bpy)$_3$]$^{2+}$ out-of-plane nearest neighbor arrangements. The dominating energy transfer pathways and mechanisms will be studied in the subsequent sections and it will be possible to understand the processes that lead to an energy harvesting at the site of lowest energy of Δ-[Os(bpy)$_3$]$^{2+}$ in {Λ-[Ru(bpy)$_3$]-Δ-[Os(bpy)$_3$]}(PF$_6$)$_4$ (see Section 5.1).

3. Emission properties and energy transfer in neat rac-[Ru(bpy)$_3$](PF$_6$)$_2$ at low temperature

3.1. ^{3}MLCT states and three different spectroscopic sites

The emission properties of the low-lying states of [Ru(bpy)$_3$]$^{2+}$ in rigid matrices have already been studied in detail and are summarized in comprehensive reviews (see [5,8,32] and compare the references [23–59]). Therefore, only a short outline is presented here. In a first approximation, the lower excited states can be related to excitations from the Ru4d-bpyπ HOMO to the bpyπ* LUMO. Thus, the resulting states are classified as MLCT states, namely as **^{1}MLCT** and **^{3}MLCT** states. The ground state is a singlet. The net transfer of electronic charge density, however, is much less than one full electron charge (for details see [5], p. 238 and [33], p. 41). At low temperature, the emissions stem from substates of a **^{3}MLCT** term, while at r.t. also a thermally activated **^{1}MLCT** emission has been identified for rac-[Ru(bpy)$_3$](PF$_6$)$_2$ [34,35].

The **^{3}MLCT** term splits according to the specific site symmetry of [Ru(bpy)$_3$]$^{2+}$ and according to spin–orbit coupling into several triplet substates (e.g. see [36–45]). In this outline, we do not discuss group-theoretical assignments, since a generally accepted classification has not yet emerged. (Compare Refs. [5], p. 175). Therefore, we designate the low-lying triplet substates observed as **I**, **II**, **III**, etc. according to their energy sequence. The totally symmetric singlet ground state is labeled as **0**. At very low temperature, for example at $T = 1.3$ K, only the lowest substates **I** and **II** emit, whereby the emission from substate **I** strongly dominates. (See Fig. 4a discussed below).

The emission properties also depend on the specific environment of the [Ru(bpy)$_3$]$^{2+}$ complex in the solid state matrix [5,46]. For example, in rac-[Ru(bpy)$_3$](PF$_6$)$_2$ the lowest electronic origin (0–0 transition of the site of lowest energy) is found at 17 809 cm^{-1}, while the lowest transition in rac-[Ru(bpy)$_3$](ClO$_4$)$_2$ lies by about 200 cm^{-1} lower in energy at 17 605 cm^{-1} [5,8,44,45]. From this dependence of the transition energy on the environment, it is expected that the lowest electronic origins of the three crystallographic [Ru(bpy)$_3$]$^{2+}$ sites in rac-[Ru(bpy)$_3$](PF$_6$)$_2$ lie at slightly different energies. Indeed, this behavior is observed and will be discussed below.

For completeness, we remark that the lowest excited states of [Ru(bpy)$_3$]$^{2+}$ in rigid crystalline phases, such as [Ru(bpy)$_3$](PF$_6$)$_2$ or [Ru(bpy)$_3$]$^{2+}$ doped into [Zn(bpy)$_3$](ClO$_4$)$_2$, are even at low temperature delocalized over the different ligands and the metal due to a relatively strong metal-induced electronic ligand–ligand coupling. (See [32,47–49] and in particular the comprehensive discussions also of alternative models in [5], p. 207). However, in fluid solutions, the situation seems to be different. Recently, McCusker et al. [50,51] have studied solvation dynamics in the femtosecond time domain. In particular, the results obtained are consistent with an initially delocalized state on the time scale of their measurement (ca. 30 fs). The system then evolves to a localized configuration, a process that appears to be coupled to non-diffusive dynamics associated with the solvent. On a longer time scale, this unsymmetrical situation develops to a distortion, which is connected with distinct nuclear shifts. Interestingly, the possibility

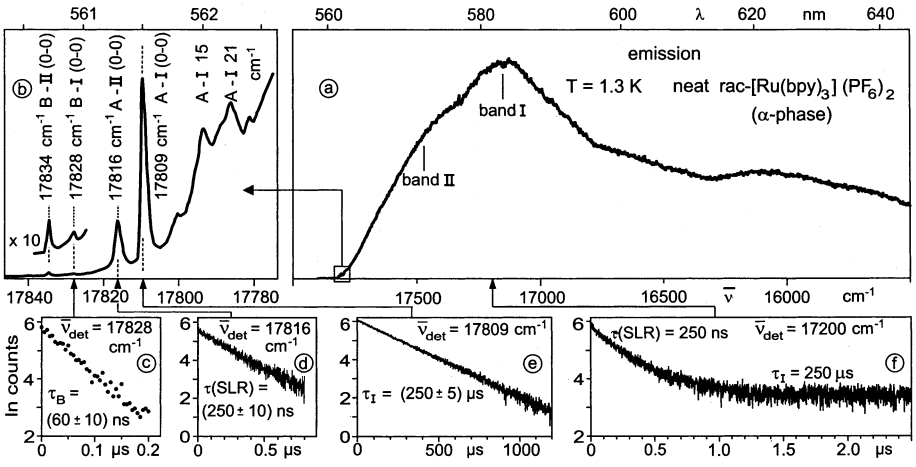

Fig. 3. Emission spectra and decay properties of neat rac-$[Ru(bpy)_3](PF_6)_2$ (α-phase) measured at $T = 1.3$ K. (a) Broad band emission spectrum. The bands I and II stem from ^{3}**MLCT** substates **I** and **II**, respectively, of $[Ru(bpy)_3]^{2+}$ at site A. (b) Spectral range of the electronic 0–0 transitions **I**→**0** and **II**→**0** at an enlarged scale. A and B represent different spectroscopic sites of $[Ru(bpy)_3]^{2+}$. (c) Emission decay of the energetically higher lying site B. τ_B is determined by the radiationless energy transfer from site B to site A in the neat material. (d) Emission decay τ(SLR) of the triplet substate **II** (site A) determined by spin-lattice relaxation (SLR). (e) Usual emission decay time τ_I of triplet substate **I** of site A. (f) Biexponential emission decay due to superimposed emissions from the substates **I** and **II** of site A of $[Ru(bpy)_3]^{2+}$. (Compare Ref. [5].)

of a solvent induced localization has been proposed nearly two decades ago by our research group [52, p. 6589].

3.1.1. Emission spectra of site A ($[Ru(bpy)_3]^{2+}$)

The emission of rac-$[Ru(bpy)_3](PF_6)_2$ (α-phase) stems dominantly from the crystallographic site of lowest energy designated as site A(Ru). Fig. 3a shows the emission spectrum measured at $T = 1.3$ K. It is not well resolvable, apart from the high-energy range, where one finds electronic origins (0–0 transitions). (See the enlarged range in Fig. 3b). From these line structures, one can identify the two lowest triplet substates **I** and **II** [5,8,53] of site A(Ru). Therefore, these states are designated as **I**(A) and **II**(A). The corresponding electronic transitions lie at 17 809 and 17 816 cm^{-1} and are separated by (6.9 ± 0.2) cm^{-1} [5,8]. A further triplet substate **III**(A) is observed at 17 870 cm^{-1}, being 61 cm^{-1} above substate **I**(A) (spectrum not reproduced) ([8] and [5], p. 177). With respect to the splitting of the ^{3}MLCT term into substates and their splitting pattern it should also be referred to Crosby's pioneering work [36,54–58]. Fig. 4a shows the energy level diagram for the low-lying triplet substates **I**(A), **II**(A), and **III**(A) of site A(Ru).

The broad emission bands displayed in Fig. 3a result from superpositions of many different vibrational satellites and their combinations with lattice modes (phonons). It has been shown that band I and II stem from the triplet substates **I**(A) and **II**(A), respectively. The occurrence of these separate bands is a consequence of different vibronic coupling properties of the substates **I**(A) and **II**(A) (e.g. see [5], p. 187). It is worth

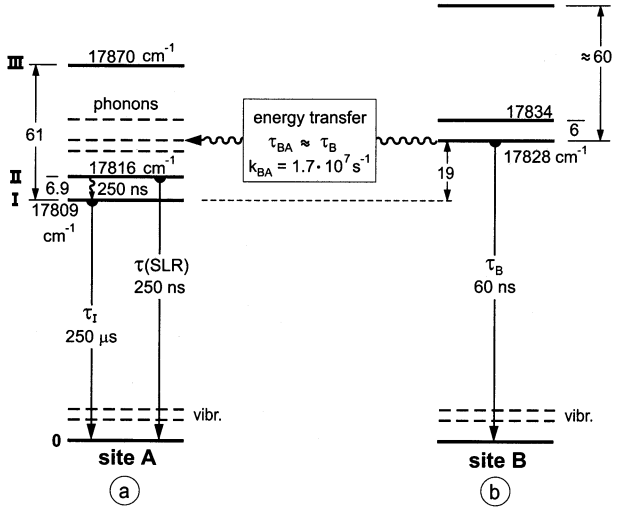

Fig. 4. Energy level diagrams for the lowest ^{3}**MLCT** substates of two spectroscopic sites, namely (a) of site A and (b) of site B of $[Ru(bpy)_3]^{2+}$ in rac-$[Ru(bpy)_3](PF_6)_2$ (α-phase). The decay and relaxation time constants are given for $T = 1.3$ K. The SLR time τ(SLR) = 250 ns has only been determined for site A(Ru). The energy position of substate **III** of site B is only estimated. The short decay time τ_B measured for site B(Ru) is determined by an energy transfer process from site B(Ru) to site A(Ru). (Compare Refs. [5,65]).

mentioning that the structure appearing in the broad band spectrum does not represent a vibrational Franck–Condon (FC) progression as has occasionally been assumed. In contrast, the structure can be traced back to combinations of vibrations with different energies, as has been demonstrated for $[Ru(bpy)_3]^{2+}$ doped into $[Zn(bpy)_3](ClO_4)_2$ [59]. In this compound, the maximum Huang–Rhys parameter for vibrational satellites is as

low as $S_{max} = 0.1$ (see [59] and [5], p. 186). This value is much too small to allow for a pronounced FC progression (e.g. see [60], p. 197).

3.1.2. Emission decay properties of site A ($[Ru(bpy)_3]^{2+}$)

The emission decay time of the lowest triplet substate **I**(A) can be recorded directly, when the electronic origin **I**(A)→**0**(A) at 17 809 cm^{-1} is selected as detection energy. At $T = 1.3$ K, one finds a strictly monoexponential decay with a time constant of $\tau_I = (250 \pm 5)$ μs (Fig. 3e). However, when the detection energy is chosen to lie at the electronic origin **II**(A)→**0**(A) at 17 816 cm^{-1}, one observes a decay time of (250 ± 10) ns (Fig. 3d). This time constant is not related to the usual radiative and non-radiative decay processes from substate **II**(A) to the ground state. But it is determined by a relaxation process, the SLR, from substate **II**(A) to the lower lying substate **I**(A). This process is controlled by the coupling strength of the two electronic states involved to the lattice and by the density of phonon/lattice states. At low temperature and an energy separation of a few cm^{-1}, the SLR time constant can be as long as several microseconds also in organometallic compounds. Processes and mechanisms of SLR have been studied in detail and are well described since several decades (e.g. see [60–62]). But the significance of these processes also for organometallic compounds has been recognized only recently by Yersin et al. [47] (See also the recent review [63]). In particular, for $[Ru(bpy)_3]^{2+}$ it has been shown [5,63] that the SLR from substate **II**(A) to substate **I**(A) with a time constant of $\tau(SLR) = 250$ ns at $T = 1.3$ K is determined by a *direct process* (compare [60–62]).

It is an important consequence of the relatively slow SLR from state **II**(A) to the lower lying state **I**(A) of $[Ru(bpy)_3]^{2+}$ that the emission of the second excited state **II**(A) cannot be frozen out, even when cooled down to $T = 1.3$ K ([5], p. 195 and [63]). Substate **II**(A) decays (approximately) with the time constant of SLR. (Fig. 3d)

For completeness it is mentioned that in general, one does not have direct experimental access to the emission decay time τ_{II} which is given by the radiative and non-radiative processes from the higher lying substate **II**(A) to the ground state **0**. However, this time constant can be determined indirectly from the temperature dependence of the long lived decay component, i.e. after thermal equilibration between the lower lying triplet substates is attained (e.g. see Refs. [44,45,55,64]). This procedure has also been carried out for $[Ru(bpy)_3]^{2+}$ doped into $[Zn(bpy)_3](ClO_4)_2$, and one obtains an emission decay time for substate **II**(A) of $\tau_{II} = 8$ μs ([5], p. 185, compare also [63]).

If the emissions of the two states **I**(A) and **II**(A) are spectrally not separated, which necessarily is the case when the detection is carried out in the spectral region of the unresolved and overlapping emission bands, one finds a biexponential decay with the two decay constants of $\tau(SLR) = 250$ ns and of $\tau_I = 250$ μs. (Fig. 3f)

Fig. 4a displays the various time constants observed at $T = 1.3$ K for site A of rac-$[Ru(bpy)_3](PF_6)_2$.

3.1.3. Electronic 0–0 transitions and emission decay time of site B ($[Ru(bpy)_3]^{2+}$)

Interestingly, an emission of a second site (site B(Ru)) is also observed [65]. Fig. 3b displays two additional, very weak electronic origins lying 19 and 18 cm^{-1}, respectively, above the corresponding 0–0 transitions of site A(Ru). The emission intensities found for these lines are by more than one order of magnitude smaller than the intensities observed for site A(Ru). Moreover, one finds a different intensity ratio and a significantly shorter decay time at these higher lying lines. Specifically, when detected at the electronic origin of the **I**(B)→**0**(B) transition at 17 828 cm^{-1}, one obtains a decay time of $\tau_B = (60 \pm 10)$ ns (Fig. 3c). This behavior is rationalized by the occurrence of a radiationless energy transfer from site B(Ru) to site A(Ru) (see Section 3.2 and [65]). Fig. 4b displays the energy level diagram and the decay time observed for site B(Ru). (The energy position of substate **III**(B) is only estimated).

3.1.4. Site C ($[Ru(bpy)_3]^{2+}$)

A careful search for emission or excitation peaks corresponding to the third crystallographic site (site C(Ru)) was not successful. According to a comparison with results found for $[Os(bpy)_3]^{2+}$ doped into rac-$[Ru(bpy)_3](PF_6)_2$, one can estimate the transition energies also for this site (Section 4.1 and [65]). The electronic origins should be about 20 cm^{-1} above those of site B(Ru). Presumably, the emission of site C(Ru) is effectively quenched by energy transfer (see below), and the weak absorptions are hidden below the much stronger absorptions of site A(Ru) in the corresponding spectral range [65].

The energies of the low-lying electronic states of the three different sites are summarized in Table 1. A

Table 1
Lowest ^{3}**MLCT** substates of $[Ru(bpy)_3]^{2+}$ and $[Os(bpy)_3]^{2+}$ in neat rac-$[Ru(bpy)_3](PF_6)_2$ [65,66]

Site	$[Ru(bpy)_3]^{2+}$		$[Os(bpy)_3]^{2+}$ [a]		
	I	**II**	**I**	**II** [b]	**III** [b]
A	17 809	17 816	14 423	14 432	14 495
B	17 828	17 834	14 460	14 465	14 521
C	(17 848) [c]	(17 854) [c]	14 496	14 503	14 566

[a] See also Section 4.1 and Fig. 5.
[b] In previous publications [5,65,66], the states **II** and **III** of $[Os(bpy)_3]^{2+}$ were designated differently, namely as **Γ** and **II**.
[c] Value estimated, compare [65].

correlation of the three crystallographic sites (Fig. 1) to the spectroscopic sites A, B and C has not yet been carried out. However, a number of spectroscopic properties seem to allow us to present a tentative correlation. (See Sections 3.2 and 4.3)

3.2. Radiationless energy transfer between different sites in rac-$[Ru(bpy)_3](PF_6)_2$

3.2.1. Energy transfer from site B ($[Ru(bpy)_3]^{2+}$) to site A ($[Ru(bpy)_3]^{2+}$)

The emission decay time measured at the lowest electronic origin **I**(B)→**0**(B) (17 828 cm^{-1}) of site B of $[Ru(bpy)_3]^{2+}$ is with $\tau_B = (60 \pm 10)$ ns by a factor of about 4×10^3 shorter than the emission decay time of 250 μs of site A (Fig. 3c and e). Therefore, this short decay cannot be explained to be determined simply by the transition from the lowest excited state **I**(B) to the ground state of an isolated site B(Ru). (The corresponding decay time τ_I(B) is of the order of 250 μs). It is more reasonable to ascribe this short lifetime τ_B to be controlled by a radiationless energy transfer from site B(Ru) to site A(Ru) with a time constant of τ_{BA}. Due to $\tau_B = (1/\tau_{BA} + 1/\tau_I(B))^{-1} \approx \tau_{BA}$, one obtains the transfer rate of $k_{BA} = 1/\tau_{BA} = 1.7 \times 10^7$ s^{-1}. This rate is relatively small, and thus the emission of site B(Ru) is not totally quenched. The smallness can be rationalized, when it is taken into account that the energy transfer is non-resonant with an energy mismatch of 19 cm^{-1} (Fig. 4).

According to the crystal structure of rac-[Ru(bpy)$_3$](PF$_6$)$_2$ (Fig. 1) these two sites are nearest neighbors and thus one would expect to have at least a small overlap of the tails of the ^{3}MLCT wavefunctions. Consequently, an energy transfer due to the Dexter exchange mechanism [67] is more probable, than a significant contribution according to the Förster dipole–dipole transfer mechanism ([68] and [69], p. 302). This is due to the extremely small transition probabilities of the electronic transitions involved. (The molar extinction coefficients for the **0**→**I** and **0**→**II** 0–0 transitions are ε (**0**→**I**) ≈ 0.02 l mol^{-1} cm^{-1} and ε (**0**→**II**) ≈ 5 l mol^{-1} cm^{-1}, respectively [8], p. 206).

It is worth mentioning that emission decay and rise times, respectively, of the same order of τ_B, namely of 20 ns, have been reported to be measured for $[Ru(bpy)_3]^{2+}$ doped into $[Zn(bpy)_3](ClO_4)_2$ [70]. This time constant fits well to a process of energy transfer between nearest neighbors of $[Ru(bpy)_3]^{2+}$ in aggregates that are formed in the process of crystal growing of this doped material (see [5], p. 199 and [32], p. 339). However, in [70] and also more recently in [71] the authors ascribe this time constant of 20 ns to an extremely slow intra-molecular ligand–ligand transfer. Usually intra-molecular energy transfer processes are by orders of magnitude faster (e.g. see [5], p. 170 and [72]). Arguments or even a physical model for the occurrence of such a weak ligand–ligand coupling that would necessarily be connected with the slow and inefficient intra-molecular transfer process are not given in Refs. [70,71]. The presentation of a corresponding model will be particularly difficult, since the ^{3}**MLCT** substates involved can be traced back to the same Ru4d orbitals, which necessarily provide a significant ligand–ligand coupling. (See the discussions of alternative models in Ref. [5], p. 207 and compare [49]).

As already mentioned in the preceding section, the emission intensity ratios at the electronic origins are different for the two sites A(Ru) and B(Ru) (Fig. 3b). At $T = 1.3$ K, the emission of site B stemming from the lowest excited state **I**(B) is quenched more effectively by energy transfer than the emission of the corresponding second excited state **II**(B). This is due to the slow equilibration between the two states **I**(B) and **II**(B), given by the SLR time of τ(SLR) ≈ 250 ns (as determined for site A(Ru)). This time is by a factor of more than 4 longer than the decay time of state **I**(B) with τ_B = 60 ns. Consequently, the emission of state **I**(B) is quenched more effectively than populated via substate **II**(B). Clearly, the relation of these time constants has a drastic influence on the intensity ratio. Therefore, one observes a higher ratio of emission intensities of origin I(A) relative to origin II(A), as compared with the corresponding intensities of site B. (Substate **I**(A) with a decay time of $\tau_I = 250$ μs is not quenched by energy transfer).

3.2.2. Energy transfer from site C ($[Ru(bpy)_3]^{2+}$) to the sites A and B ($[Ru(bpy)_3]^{2+}$)

It is expected that the electronic origins of a third spectroscopic site C(Ru) lie about 20 cm^{-1} higher in energy than those of site B(Ru) (Ref. [65] and Table 1). However, this site C(Ru) has not yet been identified spectroscopically. Presumably, the weak absorption of site C(Ru) is hidden below the absorption in particular of site A(Ru) and the emission is quenched due to energy transfer processes from site C(Ru) to the two sites A(Ru) and B(Ru) (Compare Section 3.1).

3.2.3. Energy migration along sites A ($[Ru(bpy)_3]^{2+}$)

The energy transfer from site A(Ru) to another $[Ru(bpy)_3]^{2+}$ complex sitting on an equivalent site A(Ru) (migration) is not very efficient, as can be concluded from doping experiments. Concentrations of $[Os(bpy)_3]^{2+}$ in rac-$[Ru(bpy)_3](PF_6)_2$ of more than 20% are required to quench the $[Ru(bpy)_3]^{2+}$ emission of site A completely [6] (See also Section 4.2). This behavior seems to be a consequence of small energy mismatches between formally equivalent A(Ru) sites. Thus, nearest neighbors of $[Ru(bpy)_3]^{2+}$ on A sites are normally not in resonance. This is due to the inhomogeneous distribution of the $[Ru(bpy)_3]^{2+}$ complexes and consequently of the transition energies. The inhomogeneous

line width is about 3 cm^{-1} (see Fig. 3b). Nevertheless, an effective energy transfer could, at least in principle, still occur by thermally activated hopping processes. These should lead to a pronounced temperature dependence of the quenching efficiency of the emission by impurity centers, such as $[Os(bpy)_3]^{2+}$ complexes. However, at least up to $T = 4.2$ K, these thermally activated processes are not significant (see Section 4.2). Presumably, the transfer processes are inefficient because of the very low density of phonon states in this energy range of k_BT at $T \approx 4$ K (compare Refs. [60], p. 466 and [24]).

Possibly, the small migration rate observed indicates larger spatial separations between equivalent A sites of $[Ru(bpy)_3]^{2+}$. Specifically, this is realized, when neighboring A(Ru) sites belong to two different columns (Fig. 1 and Section 2.1). Interestingly, if this explanation holds, a correlation of the spectroscopic site A(Ru) to one specific crystallographic sites is feasible.

4. Emission of Δ-$[Os(bpy)_3]^{2+}$ doped into rac-$[Ru(bpy)_3](PF_6)_2$ and energy transfer

4.1. Low lying states of $[Os(bpy)_3]^{2+}$ and three emitting sites

The lowest excited energy term of $[Os(bpy)_3]^{2+}$ is assigned in general agreement as **^{3}MLCT**. This term results in a first approximation from excitations from the Os5d-bpyπ-HOMO to the bpyπ*-LUMO [6–8,26,37–39,66,73–86] and [5], p. 212 ff. According to spin–orbit coupling and the symmetry of the complex at the individual site the **^{3}MLCT** term splits into substates. In the present investigation, we are mainly interested in properties of the lowest substates of $[Os(bpy)_3]^{2+}$. These are designated similarly as for $[Ru(bpy)_3]^{2+}$ according to their energy sequence as **I**, **II**, **III**, etc. and the singlet ground state as **0**. We are also interested in processes of energy transfer occurring in this doped material.

A deeper understanding of the electronic structure requires the information that is obtainable from highly resolved spectra. When $[Os(bpy)_3]^{2+}$ is doped into adequate matrices, such as $[Zn(bpy)_3](ClO_4)_2$ [5,84], $[Ru(bpy)_3](ClO_4)_2$ [81,82], rac-$[Ru(bpy)_3](PF_6)_2$ [5–8,26,66,83], rac-$[Ru(bpy)_3](AsF_6)_2$ [66], and rac-$[Ru(bpy)_3](SbF_6)_2$ [66], the situation is favorable. For all of these matrices, the energies of the lowest guest states are far below those of the hosts and one obtains highly resolved emission and excitation spectra. In particular, rac-$[Ru(bpy)_3](PF_6)_2$ is transparent below $\approx 17\,800$ cm^{-1} and thus provides a spectral window of more than 3300 cm^{-1} above the lowest electronic state of $[Os(bpy)_3]^{2+}$ [5,66].

Fig. 5 displays the 1.3 K emission spectrum of rac-$[Ru(bpy)_3](PF_6)_2$ (α-phase) doped with 1% Δ-$[Os(bpy)_3]^{2+}$. Obviously, for the excitation energy chosen (21 839 cm^{-1} (457.9 nm)), the emission spectrum consists of two components, which are spectrally relatively well separated. Above $\approx 14\,500$ cm^{-1}, one finds the broad band emission of the host material dominantly resulting of site A(Ru) (see Section 3.1). Below this energy of $\approx 14\,500$ cm^{-1} the Δ-$[Os(bpy)_3]^{2+}$ guest molecules emit. Interestingly, this low-energy part of the spectrum is very well resolved. But it is complicated, since it is built up from overlapping emissions of the three different sites of Δ-$[Os(bpy)_3]^{2+}$, designated as sites A(Os), B(Os), and C(Os). Moreover, these emissions exhibit pronounced vibrational satellite structures [5,8,26,66,83]. The same spectrum of Δ-$[Os(bpy)_3]^{2+}$ is obtained, when the excitation energy lies below the absorption range of the host material and when only Δ-$[Os(bpy)_3]^{2+}$ complexes are excited, for example, by use of a HeNe laser ($\lambda_{exc} = 632.8$ nm (15 803 cm^{-1})) [6,66].

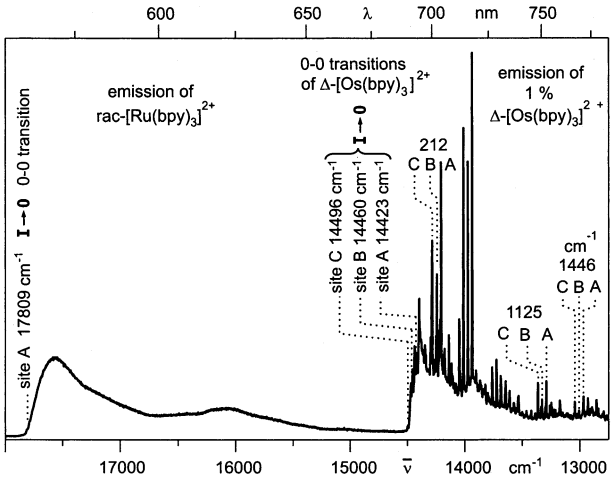

Fig. 5. Emission of rac-$[Ru(bpy)_3](PF_6)_2$ (low temperature α-phase) doped with 1% Δ-$[Os(bpy)_3]^{2+}$ (mol/mol) ($T = 1.3$ K, $\lambda_{exc} = 457.9$ nm). The lowest electronic origins of the different emitters are indicated. The emission of Δ-$[Os(bpy)_3]^{2+}$ stems from three different sites A(Os), B(Os), and C(Os), while the spectrum of rac-$[Ru(bpy)_3](PF_6)_2$ is essentially determined by the lowest site A(Ru) (see Fig. 3b). (Compare Ref. [26]).

Obviously, the Δ-$[Os(bpy)_3]^{2+}$ guest molecules can occupy all three possible crystallographic sites being available in the α-phase of the host material. However, according to the specific building principle of the host crystal structure (Section 2), Δ-$[Os(bpy)_3]^{2+}$ can replace only every second host complex of a column. Consequently, the guest molecules cannot exhibit the relatively strong intra-column contacts. Only the weaker in-plane contacts are possible [26]. Therefore, guest–guest interactions have a different quality as compared with racemic doping and with neat rac-$[Os(bpy)_3](PF_6)_2$, respectively (see also Section 4.3).

For completeness, it is mentioned that the emission spectrum of Fig. 5 is very similar to the one found for

low doping concentrations of rac-$[Os(bpy)_3]^{2+}$ guest complexes [5,6,66]. Apparently, in this situation guest–guest interactions are not yet significant. Further, by use of site-selective excitation, applying a suitably tuned laser, one can selectively excite the lowest site A(Os) and obtains a remarkably simplified one-site emission spectrum. Similarly, also an excitation spectrum of site A(Os) has been measured. From this information, a detailed knowledge about the lowest excited states of $[Os(bpy)_3]^{2+}$ (see Ref. [5], fig. 25) and about their individual vibronic coupling properties [5], p. 218 has emerged [5,8,66,83] (Compare also Section 5). Moreover, the energy positions of the lower lying triplet substates of the three spectroscopic sites could also be determined. In particular, the lowest electronic origins corresponding to the 0–0 transitions $\mathbf{0}\leftrightarrow\mathbf{I}$ lie at 14 423 cm^{-1} (site A(Os)), 14 460 cm^{-1} (site B(Os)), and 14 496 cm^{-1} (site C(Os)) (Fig. 5) [66]. Transition energies for several triplet substates of the three crystallographic sites are summarized in Table 1. We remark that the occurrence of three sites in rac-$[Ru(bpy)_3](PF_6)_2$ has been reported in Ref. [66] long before the low-temperature crystal structure of rac-$[Ru(bpy)_3](PF_6)_2$ has been published [29]. This was possible by use of $[Os(bpy)_3]^{2+}$ as spectroscopic probe. The occurrence of three sites could only be proven by applying optical high-resolution techniques.

In the present investigation, we do not report on detailed assignments, such as energy level diagrams, vibrational satellite structures, vibronic coupling properties, etc. which have been worked out by use of site-selective spectroscopy (Compare the review [5], p. 212 ff). Here, we present a different and new approach that allows us to elucidate properties of $[Os(bpy)_3]^{2+}$ namely by use of the new {Λ-$[Ru(bpy)_3]$ Δ-$[Os(bpy)_3]$}$(PF_6)_4$ compound. In this system, application of site-selective spectroscopy is not necessary, since the system shows 'self-site-selectivity' with respect to the lowest site of Δ-$[Os(bpy)_3]^{2+}$ (site A(Os)) (See [26] and Section 5).

4.2. Radiationless energy transfer and energy migration in rac-$[Ru(bpy)_3](PF_6)_2$ at low doping concentration of Δ-$[Os(bpy)_3]^{2+}$

At low concentration of Δ-$[Os(bpy)_3]^{2+}$ in rac-$[Ru(bpy)_3](PF_6)_2$ (α-phase), the excitation energy is predominantly absorbed by the $[Ru(bpy)_3]^{2+}$ host material, even when an excitation wavelength is chosen at which both compounds absorb (e.g. at $\lambda_{exc} = 457.9$ mm (21 839 cm^{-1})). Subsequently, excitation energy is transferred radiationlessly from the host (donor) to the Δ-$[Os(bpy)_3]^{2+}$ guest complexes (acceptors). The occurrence of radiationless processes is concluded from the following observations:

1) The emission intensity of the host material is strongly reduced, when $[Os(bpy)_3]^{2+}$ dopants are present. For example, doping of 0.1, 1 and 2%, quenches the emission intensity of the host material (at $T = 1.3$ K) by ≈30, ≈60 and ≈85%, respectively, compared with neat rac-$[Ru(bpy)_3](PF_6)_2$ [87,88].
2) Doping of Δ-$[Os(bpy)_3]^{2+}$ also alters the emission spectrum of the host material. This has already been demonstrated in Refs. [6,7]. The effect is also seen, when the emission spectrum of Fig. 3a is compared with the spectral component of the donor emission (above ≈14 500 cm^{-1}) of Fig. 5. In particular, the emission of the broad band I resulting from substate **I** of site A(Ru) in the rac-$[Ru(bpy)_3](PF_6)_2$ host material is quenched with increasing concentration of the dopant [6,7].
3) The emission decay time of the host material is significantly reduced by doping of Δ-$[Os(bpy)_3]^{2+}$, and the emission decay becomes multi-exponential. The long decay component decreases from 250 μs (decay time of substate **I**(A) of neat α-rac-$[Ru(bpy)_3](PF_6)_2$ at $T = 1.3$ K, Fig. 4) to 225 μs (0.1% $[Os(bpy)_3]^{2+}$), to 110 μs (1%), and to 75 μs (2%) [87,88] (Compare also [6]).
4) When the excitation wavelength of $\lambda_{exc} = 457.9$ nm is chosen, at which mainly rac-$[Ru(bpy)_3](PF_6)_2$ is excited due to the high concentration of the host material, the decay of the Δ-$[Os(bpy)_3]^{2+}$ emission is longer than its intrinsic decay time and very similar to that of the host material, since the donor is representing a long-lived reservoir. By use of a selective excitation of Δ-$[Os(bpy)_3]^{2+}$, for example with $\lambda_{exc} = 675$ nm (14 815 cm^{-1}), one obtains the much shorter decay time of the dopant itself of $\tau = (22 \pm 0.5)$ μs (decay time of substate **I** at $T = 1.3$ K, compare also Ref. [84]).

The properties described above can be rationalized by taking into account two processes of energy transfer: (1) donor–donor processes of excitation transfer by migration or hopping and (2) processes of donor–acceptor radiationless energy transfer.

4.2.1. Donor–donor transfer/migration

Obviously, donor–donor transfer or migration is not very efficient, since one needs relatively high acceptor concentrations (>20% mol/mol [6]) to quench the donor emission totally (at $T = 1.3$ K). This high concentration should be compared with other single-crystal compounds, in which already several orders of magnitude smaller amounts of dopant concentrations quench the donor emission (e.g. compare [89,90]). Some information concerning individual donor–donor transfer processes is available and has already been discussed in Section 3.2. In particular, 'down-hill' nearest neigh-

bor transfer within the host material from site C(Ru) to the sites A(Ru) and B(Ru) is fast compared with the transfer from site B(Ru) to site A(Ru). The time constant of this latter process could be determinated to $\tau_{BA} = 60$ ns corresponding to a rate of $k_{BA} = 1.7 \times 10^7$ s^{-1}. After these down-hill one- or two-step processes of energy transfer to site A(Ru) have occurred, migration processes between equivalent sites A(Ru) seem to be slow. Moreover, it is indicated that even thermally activated hopping processes do not become important with temperature increase from $T = 1.3$ to 4.2 K. In particular, doping of $[Os(bpy)_3]^{2+}$ with different concentrations up to $\approx 2\%$ lead to the same quenching effect of the host emission for $T = 1.3$ and 4.2 K, respectively [87,88].

4.2.2. Radiationless energy transfer from $[Ru(bpy)_3]^{2+}$ to $[Os(bpy)_3]^{2+}$

Radiationless energy transfer from an excited $[Ru(bpy)_3]^{2+}$ donor to an $[Os(bpy)_3]^{2+}$ acceptor in its ground state can occur as resonance process, since the donor emission (e.g. see Fig. 3a) overlaps nearly in the whole emission range with the acceptor absorption (e.g. see [74] and [5], fig. 22]). Thus, the spectral overlap integral [67–69] is non-zero and the energy transfer can be efficient. Of course, the transfer rate depends strongly on the individual separation between donor and acceptor and their mutual arrangements. For nearest neighbors in the same column with pronounced contact of Λ-$[Ru(bpy)_3]^{2+}$ with Δ-$[Os(bpy)_3]^{2+}$ (Section 2), it is expected that the tails of the electronic wavefunctions exhibit at least a small overlap. Thus, it is most likely that the Dexter exchange mechanism [67] will dominate and quench the donor emission of this type of nearest neighbor effectively.

On the other hand, for larger donor–acceptor separations, the Förster dipole–dipole transfer [68] will be of importance. Indeed, this has already been proposed according to two different and independent low-temperature studies [24,88]. Interestingly, both investigations based on different crystalline materials, namely $[Zn_{1-x-y}Ru_xOs_y(bpy)_3](ClO_4)_2$ [88] and $[Zn_{1-x-y}Ru_xOs_y(bpy)_3]$–$[NaAl(ox)_3]$ [24] (with ox = $C_2O_4^{2-}$ and x, y of the order of 0.01), provided the same estimates for the critical distance of energy transfer of $R_c \approx 30$ Å. R_c is defined according to the following equation (e.g. see [24,60])

$$k_{ET}(R_{DA}) = 1/\tau_D(R_c/R_{DA})^6 \quad (1)$$

In particular, at a donor–acceptor separation of $R_{DA} = R_c$ the energy transfer rate k_{ET} is equal to the emission decay rate $1/\tau_D$ of the donor without energy transfer.

A numerical estimate for the $[Ru(bpy)_3]^{2+}$–$[Os(bpy)_3]^{2+}$ system seems to be instructive: If an overlap of the electronic wavefunction tails can be neglected for nearest neighbors sitting on different columns, the Dexter mechanism is ineffective. But the transfer according to the Förster mechanism can affect the donor emission. With a donor–acceptor separation of $R_{DA} \approx 10$ Å for these neighbors and with $\tau_D = \tau_I = 250$ μs for the emission decay time of $[Ru(bpy)_3]^{2+}$ at $T = 1.3$ K, one obtains by use of eq. (1) an energy transfer rate of $k_{ET} \approx 3 \times 10^6$ s^{-1}. Interestingly, this estimated rate is approximately equal to the SLR rate between the two lowest triplet substates **I** and **II** of $[Ru(bpy)_3]^{2+}$ with $k(SLR) = 1/\tau(SLR) = 4 \times 10^6$ s^{-1} (Section 3.1, Fig. 4). This comparison shows that at least an energy transfer rate of the size estimated is required to explain the observation of a more efficient quenching of the state **I** emission as compared with the state **II** emission of $[Ru(bpy)_3]^{2+}$ (compare Fig. 3a with Fig. 5 and see above in this section).

In summary, quenching of the emission of rac-$[Ru(bpy)_3](PF_6)_2$ by Δ-$[Os(bpy)_3]^{2+}$ dopants will be controlled—at low temperature and low acceptor concentration—by different processes, namely by a one- or two-step down-hill donor–donor transfer, the Dexter exchange transfer for nearest neighbors in the same column and by the Förster dipole–dipole process for larger donor–acceptor separations.

4.3. High concentration of Δ-$[Os(bpy)_3]^{2+}$

4.3.1. Doping of 10% and 20% of Δ-$[Os(bpy)_3]^{2+}$ into rac-$[Ru(bpy)_3](PF_6)_2$ and energy transfer between different sites of Δ-$[Os(bpy)_3]^{2+}$

With increasing doping concentration of Δ-$[Os(bpy)_3]^{2+}$ in rac-$[Ru(bpy)_3](PF_6)_2$, the donor emission is increasingly quenched, but can still be observed up to more than 20% doping concentration. However, at this high doping, energy transfer between the different Δ-$[Os(bpy)_3]^{2+}$ sites A(Os), B(Os), and C(Os) can no longer be neglected as has been done in the discussion of the preceding section.

Fig. 6 reflects the importance of energy transfer between the three lowest sites of Δ-$[Os(bpy)_3]^{2+}$. In this figure, only the high energy parts of the emission spectra are reproduced for three different doping concentrations. The emission spectrum for the 1% concentration displayed in Fig. 6a on an enlarged scale corresponds to the spectrum shown in Fig. 5. In Fig. 6a, we have assigned the energy positions of the lowest electronic 0–0 transitions of Δ-$[Os(bpy)_3]^{2+}$ for the three sites (site A: **I** → **0** at 14 423 cm^{-1}, etc.) and several vibrational satellites, which belong to the respective 0–0 transitions (e.g. 212, 481 cm^{-1}). These 0–0 transitions carry only very weak intensities, but they can be clearly identified as is shown in Refs. [66,83]. Also for the 10 and 20% doping concentrations of Δ-$[Os(bpy)_3]^{2+}$, one can determine the electronic origins. They are also observed as very weak peaks (Figs. 6b and c). Their

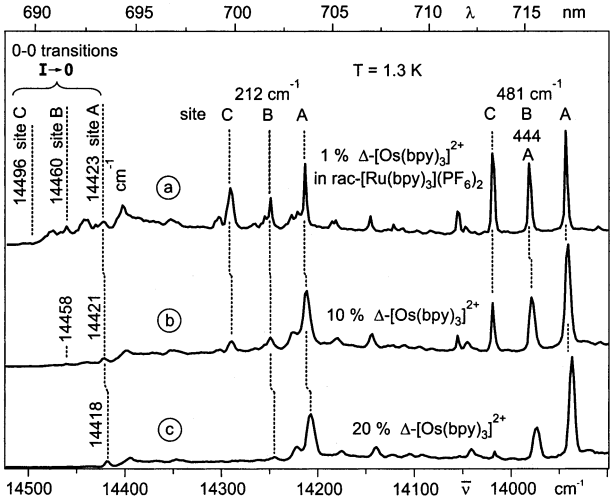

Fig. 6. Emission spectra of (a) 1%, (b) 10%, and (c) 20% Δ-$[Os(bpy)_3]^{2+}$, respectively, doped into rac-$[Ru(bpy)_3](PF_6)_2$. ($T = 1.3$ K, non-selective excitation at $\lambda_{exc} = 632.8$ nm (15 803 cm^{-1})). The electronic 0–0 transitions between the lowest triplet substates **I** and the respective electronic ground states **0** as well as several vibrational satellites are indicated. The spectra are only reproduced for the high energy regions of the emissions.

energy positions fit well (within ± 2 cm^{-1}) to the energies of vibrational satellites, when the slightly different vibrational energies as determined for {Λ-$[Ru(bpy)_3]$ Δ-$[Os(bpy)_3]$}$(PF_6)_4$ are used for comparison (compare Section 5.2).

With increasing doping concentration from 1 to 10 and 20% of Δ-$[Os(bpy)_3]^{2+}$, respectively, one observes obvious changes of the emission spectra. In particular, several phonon satellites in the region of the electronic origins (between about 14 400 and 14 500 cm^{-1}) and several vibrational satellites become much less intense or even disappear. This behavior is attributed to a selective quenching of the emissions that stem from the higher lying sites C(Os) and B(Os). For example, decreasing intensities of the corresponding 212 cm^{-1} satellites are clearly seen in the sequence of the spectra from Fig. 6a–c. Further, in the region of the 481 cm^{-1} satellites, one finds for 1% doping (Fig. 6a) that at the transition energy of 13 979 cm^{-1} the vibrational satellite of 481 cm^{-1} of site B(Os) lies at the same energy as the 444 cm^{-1} satellite of site A(Os). As with increasing doping concentration the intensity of site B(Os) is quenched due to energy transfer, the 481 cm^{-1} component vanishes, and the Δ-$[Os(bpy)_3]^{2+}$ spectrum becomes nearly a one-site spectrum, namely the one of site A(Os) (Fig. 6c). This latter aspect is even more pronounced for {Λ-$[Ru(bpy)_3]$ Δ-$[Os(bpy)_3]$}$(PF_6)_4$. Details of electronic and vibronic properties of this compound will be discussed in Section 5.

The emission decay time measured at energies of the vibrational satellites of different Δ-$[Os(bpy)_3]^{2+}$ sites is equal for all cases and amounts to (22 ± 0.5) μs (1.3 K) [91]. The value is independent of the doping concentration chosen. This behavior can be rationalized by a fast and effective energy transfer from the sites C(Os) and B(Os) to site A(Os), if they are nearest neighbors. (Nearest Δ-$[Os(bpy)_3]^{2+}$ neighbors of site A(Os) necessarily represent B(Os) and C(Os) sites. They lie in the same homochiral layer, see Section 2.2). As a consequence of this effective energy transfer, the emissions of the corresponding higher lying sites are quenched. On the other hand, a Δ-$[Os(bpy)_3]^{2+}$ site which does not have any nearest Δ-$[Os(bpy)_3]^{2+}$ neighbor is well shielded in this structure, no energy transfer occurs, and the corresponding 'isolated' Δ-$[Os(bpy)_3]^{2+}$ site emits with its intrinsic emission decay time of 22 μs.

For nearest Δ-$[Os(bpy)_3]^{2+}$ neighbors, the energy transfer mechanism can most likely be assigned as Dexter exchange [67,69] process due to the proximity of donor and acceptor. Moreover, the electric dipole transition probabilities in the resonance region of donor and acceptor sites are extremely small, at least for the B(Os) → A(Os) transfer situation. This rules out an efficient dipole–dipole transfer [68,69].

4.3.2. *Neat rac-[Os(bpy)$_3$](PF$_6$)$_2$*

It is worth mentioning that an emission spectrum of neat rac-$[Os(bpy)_3](PF_6)_2$ has also been monitored. Although, it is dominated by a broad background even at $T = 1.3$ K, one can resolve and identify the structure in the region of the lowest electronic origin and a number of vibrational satellites. (Spectrum not reproduced, but see [91]). The lowest electronic 0–0 transition between the triplet substate **I** and the ground state **0** lies at $(14\,399 \pm 3)$ cm^{-1}, where we observe a very weak transition in the emission spectrum. Further, the vibrational energies known [5,66,83] fit to energy separations between this weak transition and the vibrational satellites observed. (compare also Section 5.2). Due to the pronounced similarities of the three crystallographic structures, namely of rac-$[Ru(bpy)_3](PF_6)_2$, {Λ-$[Ru(bpy)_3]$Δ-$[Os(bpy)_3]$}$(PF_6)_4$, and of rac-$[Os(bpy)_3](PF_6)_2$ [26–31], it is expected that the latter compound undergoes also a phase transition below $T \approx 200$ K and that a resulting α-phase exhibits also three different low-temperature sites. Therefore, we assign the electronic origin observed at 14 399 cm^{-1} as spectroscopic site A of $[Os(bpy)_3]^{2+}$. Only this site A(Os) of lowest energy emits, while the emissions of the sites of higher energies are quenched by energy transfer.

Interestingly, the resolved structure of site A(Os) can only be detected for $T < 2.0$ K. Already at a slightly higher temperature, the emission is completely smeared out. Further, the fine structure can only be recorded by applying cw excitation, while application of pulsed excitation does not allow to resolve the structure, even at $T = 1.3$ K. This behavior is in contrast to the

properties of most compounds investigated so far (e.g. see [5,32,92]). Presumably, thermally activated migration/hopping processes result in a population of a very inhomogeneous distribution of $[Os(bpy)_3]^{2+}$ chromophores. The activation energy k_BT is as low as about 1 cm^{-1} and can be generated by thermal effects of the excitation pulse or by direct temperature increase. Due to the low activation energy required, the hopping processes are confined to equivalent sites A(Os), since different sites are thermally not accessible. (The energy separations for different Δ-$[Os(bpy)_3]^{2+}$ sites in rac-$[Ru(bpy)_3](PF_6)_2$ are 37 and 73 cm^{-1}, respectively, see Fig. 6). Moreover, the very effective process of smearing out the spectra with a small activation energy might be indicative of an excitation hopping within the same column. Equivalent sites that belong to the same column are only found on the specific column that passes through (00z) (Section 2.1). Thus, the tentative model suggests that the spectroscopic site A of neat rac-$[Os(bpy)_3](PF_6)_2$ (α-phase) can be identified to belong to the crystallographically specific column. In contrast, the situation for neat rac-$[Ru(bpy)_3](PF_6)_2$ (α-phase) seems to be different. It is indicated that the lowest spectroscopic site A of $[Ru(bpy)_3]^{2+}$ has its symmetry-related position on a different column. It seems to be a confirmation of this model that in the situation of rac-$[Ru(bpy)_3](PF_6)_2$ the spectral broadening effects described above do not occur (Section 3.2).

4.3.3. *Shift of the electronic transition energy with the doping concentration*

With increasing doping concentration, the transition energy between the lowest triplet substate **I** and the ground state **0** is significantly red shifted. Fig. 7 displays this effect for Δ-$[Os(bpy)_3]^{2+}$ doped into rac-$[Ru(bpy)_3](PF_6)_2$, for {Λ-$[Ru(bpy)_3]$ Δ-$[Os(bpy)_3]$}$(PF_6)_4$ and for neat rac-$[Os(bpy)_3](PF_6)_2$. Interestingly, the transition energy is directly correlated to the concentration. This shows that the sites A(Os) of the different compounds are related, including the 100% material. Obviously, the energy shifts observed are connected to concentration dependent changes of the individual environment of the $[Os(bpy)_3]^{2+}$ chromophore. However, a simple correlation between the respective lattice constants and/or unit cell volumes cannot be given. But we want to point to an investigation carried out for $[Os(bpy)_3]^{2+}$ doped into $[Ru(bpy)_3](ClO_4)_2$. It was found that by application of a high external hydrostatic pressure the lowest electronic transition is shifted by $\Delta_v^I/\Delta p = -13$ cm^{-1} $kbar^{-1}$ (at $T = 2$ K) ([5], p. 218 and

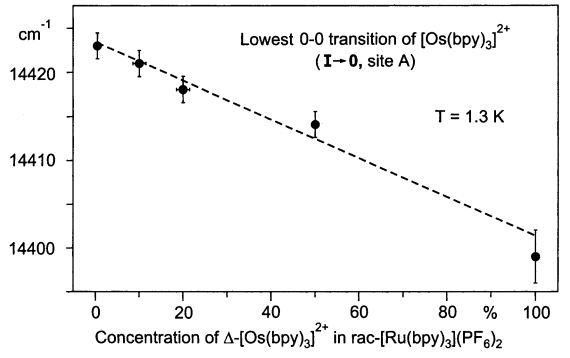

Fig. 7. Transition energies of the lowest triplet substates (**I**→**0**) of $[Os(bpy)_3]^{2+}$ doped into rac-$[Ru(bpy)_3](PF_6)_2$ for the sites of lowest energy (sites A) for different doping concentrations. The transition energies correspond to 0–0 transitions determined from emission spectra at $T = 1.3$ K. The 50 and 100% concentrations correspond to {Λ-$[Ru(bpy)_3]$Δ-$[Os(bpy)_3]$}$(PF_6)_4$ and neat rac-$[Os(bpy)_3](PF_6)_2$, respectively.

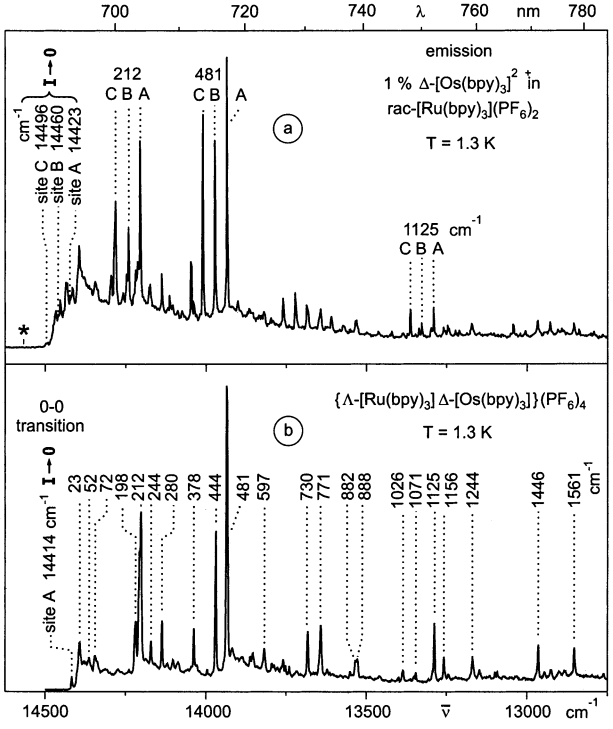

Fig. 8. (a) Emission of 1% Δ-$[Os(bpy)_3]^{2+}$ (mol/mol) doped into rac-$[Ru(bpy)_3](PF_6)_2$ ($T = 1.3$ K). The same spectrum is reproduced in Fig. 5, but here an enlarged scale is used. The intensity observed in the region of the asterisk represents the low-energy tail of the $[Ru(bpy)_3]^{2+}$ host emission. The emission below about 14 500 cm^{-1} stems from the three different sites A, B, and C of Δ-$[Os(bpy)_3]^{2+}$. (b) Emission spectrum of {Λ-$[Ru(bpy)_3]$Δ-$[Os(bpy)_3]$}$(PF_6)_4$ at $T = 1.3$ K. The emission results only from site A of Δ-$[Os(bpy)_3]^{2+}$ (site A(Os)), although the compound is non-selectively excited at $\lambda_{exc} = 457.9$ nm (21 839 cm^{-1}). Due to different processes of radiationless energy transfer, the excitation energy is effectively accumulated at this lowest site A(Os). The emission stems from the lowest ^{3}**MLCT** substate **I**. The vibrational satellite structure is Herzberg-Teller induced, all satellites represent false origins (see Fig. 10). The vibrational energies given are determined relative to the energy of the electronic 0–0 transition at 14 414 cm^{-1}. As compared with our previous study [26], we find slightly different energies, which, however, deviate only of the size of the experimental error of ±2 cm^{-1} (compare Ref. [26]).

[93]). This red shift is ascribed to be at least in part induced by a steric interaction of the chromophore with its environment (Compare [94]). Thus, the red shift observed for increasing concentration (Fig. 7) might be similarly related to more pronounced steric interactions of the $[Os(bpy)_3]^{2+}$ chromophore with its environment.

5. Energy harvesting and emission properties of {Λ-[Ru(bpy)$_3$]Δ-[Os(bpy)$_3$]}(PF$_6$)$_4$

The emission properties of the title compound are very remarkable. In Fig. 8, its low-temperature spectrum is compared with that of 1% Δ-$[Os(bpy)_3]^{2+}$ doped into rac-$[Ru(bpy)_3](PF_6)_2$. The latter one, displayed in Fig. 8a, is already reproduced in Fig. 5 and shortly discussed in Section 4.1. In particular, it has been shown that the spectrum consists of overlapping emissions that stem from three different sites A(Os), B(Os), and C(Os). In contrast, the new hetero-racemic compound exhibits a much simpler spectrum (Fig. 8b). The emission results only from one single site, namely of site A(Os). It is further very favorable that the broad emission background seen for the doped material and resulting in part from the unquenched rac-$[Ru(bpy)_3](PF_6)_2$ host, is much weaker for the title compound (compare Fig. 8b to Fig. 8a and Fig. 5).

The spectral changes observed are due to energy transfer and harvesting effects [26,27] (Section 5.1). They lead to a simpler and better resolved spectrum, as is discussed below. As consequence, the information reflected by this emission spectrum of {Λ-$[Ru(bpy)_3]$ Δ-$[Os(bpy)_3]$}$(PF_6)_4$ allows us to gain a detailed insight into the system's properties (Section 5.2). Moreover, the title material exhibits features that are only rarely observed for other compounds, namely the large-range tunability of emission properties under application of external magnetic fields. These effects are discussed in Section 5.3.

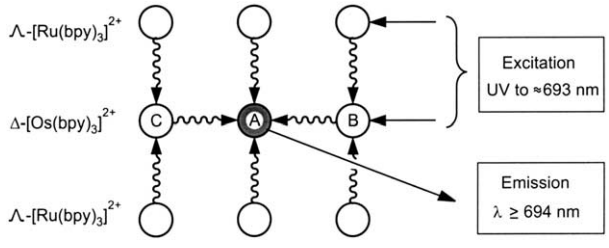

Fig. 9. Schematic and simplified diagram of absorption, radiationless energy transfer, and emission processes in {Λ-$[Ru(bpy)_3]$ Δ-$[Os(bpy)_3]$}$(PF_6)_4$ (low-temperature α-phase). Independent of the excitation energy applied, the excitation is transferred radiationlessly and with high efficiency to the site of lowest energy of Δ-$[Os(bpy)_3]^{2+}$ (site A(Os)), i.e. the excitation energy is harvested at this site. Only this site A(Os) emits. Thus, the compound exhibits the interesting property of self-site-selectivity (compare Ref. [26]).

5.1. Energy transfer and harvesting effects

The crystal structure of {Λ-$[Ru(bpy)_3]$Δ-$[Os(bpy)_3]$}$(PF_6)_4$ (α-phase) with its layered arrangement of Λ-$[Ru(bpy)_3]^{2+}$ and Δ-$[Os(bpy)_3]^{2+}$ complexes and energy transfer paths are very schematically displayed in Fig. 9 (Compare Section 2.2). In this compound very specific processes of energy transfer occur. They have already been analyzed in the preceding sections. Here, it is summarized, what happens after an excitation:

1) Excitation of a Λ-$[Ru(bpy)_3]^{2+}$ complex is followed by an effective energy transfer to a nearest neighbor of Δ-$[Os(bpy)_3]^{2+}$ in the same column, whereby the Λ-$[Ru(bpy)_3]^{2+}$ emission is quenched (see Section 4.2). The specific site of the acceptor can be each of the three different Δ-$[Os(bpy)_3]^{2+}$ sites A(Os), B(Os), and C(Os), depending on the position of the absorbing Λ-$[Ru(bpy)_3]^{2+}$ unit. Energy transfer or migration between different sites of Λ-$[Ru(bpy)_3]^{2+}$ is relatively ineffective and slow and presumably unimportant in this system (Section 3.2). But even if a one-step C(Ru) → A(Ru) transfer, for example, occurred, the excitation would subsequently also be transferred to one of the Δ-$[Os(bpy)_3]^{2+}$ sites. If this Δ-$[Os(bpy)_3]^{2+}$ acceptor site represents the site of lowest energy, namely site A(Os), an emission can take place. On the other hand, energy transfer to the acceptor sites B(Os) and C(Os) is followed by a further transfer process as is discussed subsequently.
2) An excitation of a Δ-$[Os(bpy)_3]^{2+}$ complex can either occur directly by absorption of a photon or indirectly by energy transfer. If the Δ-$[Os(bpy)_3]^{2+}$ sites B(Os) or C(Os) are involved, they act as donors and transfer their excitation energy radiationlessly to the lowest site A(Os). The emission of the two other sites B(Os) and C(Os) are effectively quenched. Consequently, again only site A(Os) can emit. (Section 4.3). Certainly, direct excitation of site A(Os) is also possible.

In summary, the excitation energy is effectively transferred to the site of lowest energy of Δ-$[Os(bpy)_3]^{2+}$ (site A), irrespectively of the individually excited site of Λ-$[Ru(bpy)_3]^{2+}$ or Δ-$[Os(bpy)_3]^{2+}$. The excitation energy is harvested at this site A of Δ-$[Os(bpy)_3]^{2+}$, and only this site A of Δ-$[Os(bpy)_3]^{2+}$ can emit (Fig. 9). The excitation energy may lie in the whole range of absorption of the title compound, namely from the UV to $\lambda_{exc} \approx 693$ nm (14 430 cm^{-1}). Due to processes of energy transfer and harvesting, the

emission is always site-selective and hence, the system exhibits the interesting property of self-site-selectivity.

5.2. Low-energy states and emission properties of Δ-[Os(bpy)$_3$]$^{2+}$ (site A)

The low-temperature emission spectrum of {Λ-[Ru(bpy)$_3$] Δ-[Os(bpy)$_3$]}(PF$_6$)$_4$ is reproduced in Fig. 8b. This spectrum is detected at $T = 1.3$ K, but at least up to $T = 4.2$ K, one does not observe any significant change. Moreover, the emission spectrum and the long-lived decay properties do not depend on whether higher lying states of Λ-[Ru(bpy)$_3$]$^{2+}$ or Δ-[Os(bpy)$_3$]$^{2+}$ are excited. The spectral resolution obtainable is much better than generally found for [Ru(bpy)$_3$]$^{2+}$ complexes. This is ascribed to a weaker coupling of [Os(bpy)$_3$]$^{2+}$ complexes to lattice/phonon modes. The emission displayed in Fig. 8b stems only from the site of lowest energy of Δ-[Os(bpy)$_3$]$^{2+}$ (site A), as is illustrated in the preceding section.

5.2.1. Lowest 0–0 transition **I**→**0**

The lowest electronic 0–0 transition from a ^{3}**MLCT** substate **I** to the singlet ground state **0** is identified to lie for site A at (14414 ± 1) cm^{-1} (Fig. 8b). As compared with the intensities of the vibrational satellites, the intensity at the electronic origin is extremely weak. The identification of this weak peak as electronic origin is based on a fit of vibrational energies ([5], p. 213 ff and [66,83]), and in particular, on the growing in of the emission intensity under application of a magnetic field exactly at this energy (Section 5.3).

The forbidden-ness of the **0**↔**I** transition at zero magnetic field, being also reflected in the relatively long emission decay time of $\tau_I = 22$ μs at $T = 1.3$ K [26], is a consequence of its singlet–triplet character (spin-selection rule) and of a symmetry restriction at this C_3 site. In particular, the importance of a symmetry forbidity is concluded from a comparison of the title compound to [Os(bpy)$_3$]$^{2+}$ doped into a [Zn(bpy)$_3$](ClO$_4$)$_2$ matrix. In this latter material, the dopant sits on a C_2 site symmetry [95,96]. As a result of the symmetry reduction from C_3 to C_2, one observes a relatively intense transition also at the purely electronic origin [5, fig. 30].

The red shift of the 0–0 transition of site A from 14423 cm^{-1} for 1% Δ-[Os(bpy)$_3$]$^{2+}$ in rac-[Ru(bpy)$_3$]-(PF$_G$)$_2$ (Fig. 8a) to 14414 cm^{-1} for Δ-[Os(bpy)$_3$]$^{2+}$ in {Λ-[Ru(bpy)$_3$] Δ-[Os(bpy)$_3$]}(PF$_6$)$_4$ (Fig. 8b) is related to steric differences in the two structures (Compare Fig. 7 and Section 4.3).

5.2.2. Vibrational satellite structure

The emission spectrum shown in Fig. 8b is dominated by a rich vibrational satellite structure, which is connected to the electronic origin **I**→**0** at 14414 cm^{-1}. The energies of the corresponding vibrational modes are specified relative to this electronic origin. The low-energy modes (e.g. 23, 52, and 72 cm^{-1}) are assigned to have significant lattice or chromophore-matrix character. In the range of higher vibrational energies up to about 500 cm^{-1} (e.g. 212, 280, 444, and 481 cm^{-1}), one finds fundamentals of metal–ligand (ML) character. Finally, fundamentals with energies higher than about 500 cm^{-1} represent internal ligand modes (e.g. 1125, 1446, 1561 cm^{-1}). For most of the more intense satellites, one also observes weak side lines, which are assigned to phonon satellites.

Interestingly, the relatively large satellite intensity in the energy range of M–L vibrational modes reflects the MLCT character of the corresponding electronic transition [33]. A more detailed analysis of the vibrational modes should be based on a normal coordinate analysis, which, however, is not yet available.

Obviously, the radiative deactivation as purely electronic transition is orders of magnitude less efficient than the radiative deactivation paths involving vibrational modes (Fig. 8b). Moreover, these satellites do not belong to vibrational FC progressions (but see Section 5.3). Therefore, it is concluded that the vibrational satellite structure observed, is induced by processes of vibronic coupling of state **I** to higher lying states (Fig. 10). This type of coupling, called Herzberg–Teller (HT) coupling [97–100,83], provides: (1) the required singlet admixture to the triplet substate **I** and (2) lifts the symmetry restrictions. Indeed, the vibrational modes involved match well to IR active vibrations ([5], table 9 and [66,83]). The corresponding coupling mechanisms are classified as spin–vibronic and spin–orbit–vibronic coupling, respectively, depending on the vibrational mode involved ([5], p. 218 and [83]). Generally, consideration of these coupling paths is of high significance for triplet emissions of organometallic compounds with

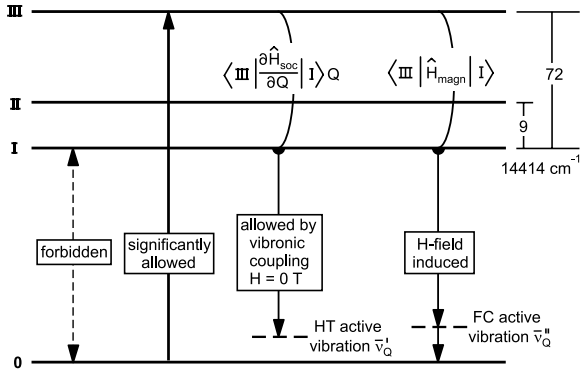

Fig. 10. Lowest excited states of Δ-[Os(bpy)$_3$]$^{2+}$ (site A) in {Λ-[Ru(bpy)$_3$] Δ-[Os(bpy)$_3$]}-(PF$_6$)$_4$ (α-phase). The matrix elements describe schematically coupling routes according to spin-vibronic coupling (as an example) and magnetic coupling, respectively. State **II** is spectroscopically not important in this respect, however, couplings to higher lying states are also possible. (HT = Herzberg–Teller, FC = Franck–Condon) (Compare Refs. [5], p. 222, [92], p. 130, and [101].) The emission decay time at $T = 1.3$ K and $H = 0$ T is $\tau = 22$ μs.

heavy central metal ions, such as Ru^{2+}, Os^{2+}, Pt^{2+}, etc. This is due to the importance of spin–orbit coupling and its modulation with adequate modes. In particular, it is easily visualized that the M–L vibrational modes are effective in this respect. The vibrations of the metal relative to the ligands can modulate the effective spin–orbit coupling and this can induce the intensities of the corresponding vibronic satellites. This mechanism, the spin–vibronic coupling path, is schematically shown in Fig. 10. A more complete description of mechanisms of vibronic coupling should also take spin–orbit–vibronic coupling into account. This latter mechanism is mainly responsible for the occurrence of vibrational satellites of internal ligand character. Due to clearness of the diagram, we do not show the corresponding matrix element in Fig. 10. (For more detailed background information see Ref. [92], p. 129).

It will be shown in Section 5.3 that by application of a high magnetic field, one can tune in FC activity.

5.2.3. Higher lying electronic states

Excitation spectra of {Λ-[Ru(bpy)$_3$]Δ-[Os(bpy)$_3$]}-$(PF_6)_4$ have been recorded at $T = 1.3$ K [91]. Due to the high optical density of the crystals, the spectral range investigated was restricted only up to about 100 cm^{-1} above the position of the lowest excited state **I** of site A(Os). Obviously, these excitation spectra do not represent site-selective spectra. Nevertheless, one can identify two further excited states of site A(Os) above triplet substate **I**(A) (14 414 cm^{-1}), namely state **II**(A) at 14 423 cm^{-1} ((9 ± 0.5) cm^{-1} above **I**(A)) and state **III**(A) at 14 486 cm^{-1} ((72 ± 2) cm^{-1} above **I**(A) (Fig. 10). Corresponding states have already been identified for 1% $[Os(bpy)_3]^{2+}$ doped into rac-$[Ru(bpy)_3](PF_6)_2$ (Table 1 and Refs. [5,66,83,101]). For completeness, it is mentioned that state **II**(A) is spectroscopically not very prominent (small radiative rate of a higher lying state, no low-temperature emission [102]), while state **III**(A) strongly influences the emission properties under magnetic field application. This is due to the large molar extinction coefficient of about 5×10^3 l mol^{-1} cm^{-1} for the **0** → **III**(A) transition [103,83].

5.3. Tuning of emission properties of Δ-$[Os(bpy)_3]^{2+}$ under application of magnetic fields

Under application of a high magnetic field, the emission spectrum changes drastically. In Fig. 11, the spectrum of site A(Os) measured at $H = 0$ T is compared with the one detected at $H = 12$ T.

5.3.1. Electronic origins

The lowest electronic 0–0 transition **I** → **0** at 14 414 cm^{-1} of site A gains an enormous intensitiy with magnetic field application. For 1% $[Os(bpy)_3]^{2+}$ in rac-$[Ru(bpy)_3](PF_6)_2$, an intensity increase of a factor

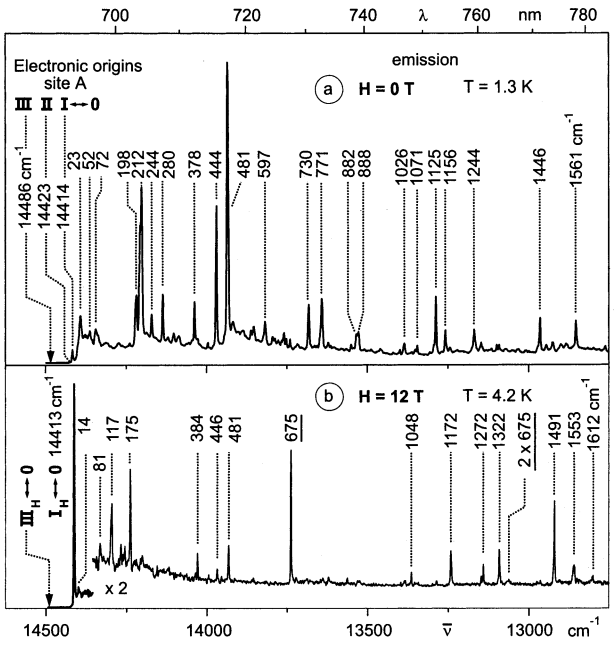

Fig. 11. (a) Emission spectrum of {Λ-[Ru(bpy)$_3$]Δ-[Os(bpy)$_3$]}$(PF_6)_4$ at $T = 1.3$ K and $H = 0$ T. This spectrum is the same as shown in Fig. 8b and is reproduced here for comparison. All vibrational satellites are induced by HT coupling. (See Fig. 10.) The three lowest electronic 0–0 transitions of site A of Δ-$[Os(bpy)_3]^{2+}$ are also indicated. Origins II and III have been determined from excitation spectra [91]. (b) Emission of the same compound, but under application of a magnetic field of $H = 12$ T ($T = 4.2$ K, $\lambda_{exc} = 457.9$ nm (21 839 cm^{-1})). With field application, the intensity of the lowest electronic 0–0 transition grows in by several orders of magnitude. The electronic origin dominates the spectrum, and the vibrational satellite structure is largely determined by FC active modes. (Compare Fig. 10). This result demonstrates that the emission properties are tunable over a wide range by application of high magnetic fields. (Compare Refs. [5,83]).

of at least 10^3 is reported for a field increase up to $H = 6$ T [83]. The magnetically induced transition $\mathbf{I}_H \rightarrow \mathbf{0}$ grows in exactly at the energy of the unperturbed and weak **I** → **0** transition (experimental error ± 0.3 cm^{-1} [102]). Only for $H > 7$ T one observes a small red shift, which increases to 1.0 cm^{-1} up to $H = 12$ T. These properties strongly support the assignment of the small peak at 14 414 cm^{-1} that is observed at zero magnetic field as electronic origin (Fig. 11a and Section 5.2).

With magnetic field increase, the second electronic transition **0** → **II** (at 14 423 cm^{-1}) gains at least two orders of magnitude less intensity than the transition **0** → **I** and is red shifted by about 1.5 cm^{-1} up to 12 T. On the other hand, the **0** → **III** transition is slightly blue shifted by ≈ 0.5 cm^{-1} up to 12 T. (These data result from excitation spectra measured for 1% rac-$[Os(bpy)_3]^{2+}$ in rac-$[Ru(bpy)_3](PF_6)_2$. [102]).

The emission intensity increase of the lowest electronic transition **0** ↔ **I** (site A) can be explained by a magnetically induced admixture of the wavefunction of a higher lying state to the wavefunction of triplet substate **I**(A). According to the behavior described

above, state **III**(A) seems to be the active candidate (Fig. 10). This state carries a high transition probability with respect to the transition to the ground state. Both perturbed states $\mathbf{I}_H$(A) and $\mathbf{III}_H$(A) exhibit a repulsive interaction under application of a high magnetic field. (State **II**(A) is unimportant in this respect, since it carries only weak allowedness.). Due to the relatively large energy separation of 72 cm^{-1} between these two states **I**(A) and **III**(A) and the small Zeeman shifts observed, the situation may be described by the low-field limit. Thus, it is reasonable to apply a simple first order perturbation model to these interactions. A corresponding treatment has already been applied to the two lowest states of rac-$[Ru(bpy)_3](PF_6)_2$ [104], and the results can directly be utilized for the present situation.

In particular, for the low-field limit, it can be deduced that the radiative rate $k_r(\mathbf{I} \leftrightarrow \mathbf{0})$, i.e. the emission intensity of the transition $\mathbf{I}_H(A) \rightarrow \mathbf{0}(A)$, should increase according to ([104,105]):

$$k_r(\mathbf{I} \leftrightarrow \mathbf{0}) = \text{const.}\ H^2 \quad (2)$$

Indeed, exactly this behavior has been observed for the 1% material. One finds that the emission intensity at the electronic origin follows a quadratical dependence of the magnetic field. Similarly, an absorption and an excitation peak, respectively, grows in ([5], p. 224 and [83]). For $\{\Lambda$-$[Ru(bpy)_3]\Delta$-$[Os(bpy)_3]\}(PF_6)_4$ an equivalent behavior is found (Fig. 11b and [91]).

First order perturbation treatment can also be used to describe the magnetic field dependence of the emission decay time $\tau_H(\mathbf{I} \rightarrow \mathbf{0})$. One obtains the following expression ([106] and [107], p. 145):

$$(1/\tau_H) - (1/\tau_0) = \text{const.}\ H^2 \quad (3)$$

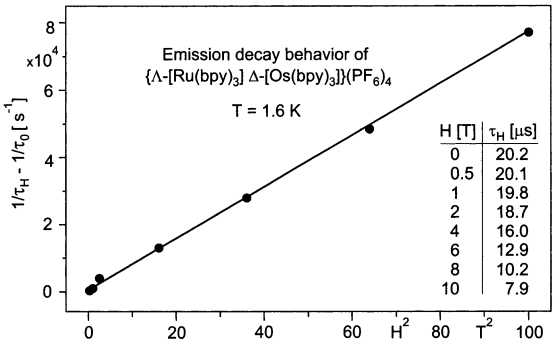

Fig. 12. By application of high magnetic fields, the emission decay time of the lowest excited state **I** of Δ-$[Os(bpy)_3]^{2+}$ (site A) is reduced. This is due to a field-induced mixing of state **I** with the higher lying state **III** having an energy separation of 72 cm^{-1} (see Fig. 10). The diagram demonstrates that the corrected emission decay rate $(1/\tau_H - 1/\tau_0)$ follow a H^2 dependence, wherein τ_H and τ_0 are the decay times with and without a magnetic field H, respectively. This quadratical field dependence is expected from a first order pertubation treatment (see eq. (3)). The experimental error in this series of decay times is about ± 0.2 μs. $\lambda_{exc} = 689.7$ nm (14 499 cm^{-1}), $\tilde{\nu}_{det} = 13\,933$ cm^{-1} (**I** → **0**–481 cm^{-1}).

For $\{\Lambda$-$[Ru(bpy)_3]\Delta$-$[Os(bpy)_3]\}(PF_6)_4$, the behavior predicted by this equation is clearly fulfilled, when the emission decay times measured at $T = 1.6$ K with and without an applied magnetic field, τ_H and τ_0, respectively, are used (Fig. 12). From this result, one can conclude [108]: (1) the low-field limit represents a good approximation to describe the magnetic field induced perturbation of triplet substate **I**(A) of the title compound. (2) Application of a magnetic field strength up to $H = 10$ T has no significant influence on the non-radiative deactivation rate. Otherwise, one should observe a clear deviation from the quadratical field dependence [106].

We remark that a magnetic field induces a very strong increase of the radiative rate, namely of the 0–0 transition $\mathbf{0} \rightarrow \mathbf{I}$, for which one finds a growing in of at least three orders of magnitude for a field increase from $H = 0$ to 6 T. However, the emission decay time is only reduced by a factor of less than two (Fig. 12). Thus, it can be concluded that the emission decay time is largely determined by non-radiative processes.

5.3.2. *Vibrational satellite structure*

The comparison of the spectra displayed in Fig. 11 shows further that the vibrational satellite structure is completely altered. In particular, the electronic origin dominates at high field as compared with the vibrational satellites. Moreover, vibrational satellites that are not found at zero magnetic field are the most intense ones at high field (e.g. 117, 175, 675, 1322, 1491 cm^{-1}) (Fig. 11b). For example, for the most prominent satellite, corresponding to the 675 cm^{-1} mode, it has been shown that it exhibits just the same intensity behavior as the electronic origin, namely one also finds an increase according to a quadratical field dependence (compare Refs. [5], p. 225 and [83]). Moreover, satellites that dominate at $H = 0$ T (Fig. 11a), such as the 212 and the 1125 cm^{-1} satellites, are relatively weak at $H = 12$ T.

These results can be rationalized, when it is assumed that all vibrational satellites growing in with significant intensity are totally symmetric FC active fundamentals. Specifically, for the 675 cm^{-1} fundamental, one observes also the second member of a FC progression at 1350 $cm^{-1} = 2 \times 675$ cm^{-1}, though not very pronounced.

The importance of a progression is often characterized by the Huang–Rhys parameter S. This value can be determined by applying the following relation (e.g. see [92], p. 133):

$$I_v / I_{v-1} = S/v \quad (4)$$

where v is the vibrational quantum number and I_v is the satellite intensity of the respective member of the FC progression. This expression is derived as low-temperature approximation for compounds with similar force

constants in the electronic ground state and the excited state [92,109,110].

For the 675 cm^{-1} progression of Δ-$[Os(bpy)_3]^{2+}$, one finds a value of $S = 0.08$. And for the other modes that grow in under application of a magnetic field the value of the S parameter is even smaller. A maximum Huang–Rhys paramater of $S_{max} = 0.08$ represents a very small value, if compared with other compounds ([60], p. 200 and [109–111,5,92]). This smallness implies that the potential hypersurface of state **I** has nearly the same equilibrium positions as that of the electronic ground state **0**. This holds also for the perturbing state **III**. (For background information see Refs. [60], p. 200, [92], p. 131, and [109–111]). Interestingly, this result reflects directly that no significant geometry change occurs, when the lowest state(s) of $[Os(bpy)_3]^{2+}$ in a rigid matrix is (are) excited. Thus, it can be concluded that a localization in the excited state does not occur (For more details, see Refs. [5], p. 229 and [84]).

6. Summary and conclusion

The newly designed crystalline {Λ-$[Ru(bpy)_3]$Δ-$[Os(bpy)_3]$}$(PF_6)_4$ material exhibits a number of interesting photophysical properties. These are directly related to the specific crystallographic structure which essentially consists of rigorously alternating homochiral layers of Λ-$[Ru(bpy)_3]^{2+}$ and Δ-$[Os(bpy)_3]^{2+}$ (or vice versa). The low temperature α-phase is characterized by three different crystallographic sites in each layer. If the compound is optically excited, different processes of inter- and intra-layer radiationless energy transfer occur. These processes are studied and analyzed by investigating: (1) the parent neat rac-$[Ru(bpy)_3](PF_6)_2$ material; (2) doped $[Ru_{1-x}Os_x(bpy)_3](PF_6)_2$ compounds, and (3) the hetero-racemic {Λ-$[Ru(bpy)_3]$Δ$[Os(bpy)_3]$}$(PF_6)_4$ system. Depending on the respective material and the individual transfer step, the Förster dipole–dipole mechanism and the Dexter exchange mechanism, respectively, has to be taken into account. The new hetero-racemic material is characterized by the specific property that the excitation energy is transferred efficiently to and accumulated at the site of lowest energy, representing a Δ-$[Os(bpy)_3]^{2+}$ complex (site A). As a consequence, only this site A emits. This behavior is independent of the excitation energy, when it is chosen in the range from the UV over the whole visible to the red up to $\lambda_{exc} \approx 693$ nm (14 430 cm^{-1}). Fig. 9 summarizes this behavior schematically.

It is a particularly interesting property of this specific structure type that the emitting Δ-$[Os(bpy)_3]^{2+}$ site is: (1) well isolated with respect to further processes of energy transfer at low temperature, (2) experiences only a weak interaction with low-energy lattice/phonon modes, and (3) is only exposed to small inhomogeneity effects in the crystallographic environment given. Consequently, one obtains highly resolved spectra of Δ-$[Os(bpy)_3]^{2+}$. These spectra lead to a detailed insight into the properties of lowest electronic states and their vibronic complex behavior. Interestingly, highly resolved spectra are obtained for all excitation wavelengths, in particular without applying the spectroscopic method of site-selectivity. This is due to the specific structure of {Λ-$[Ru(bpy)_3]$Δ-$[Os(bpy)_3]$}$(PF_6)_4$ that provides self-site-selectivity due to energy transfer and harvesting effects.

Moreover, {Λ-$[Ru(bpy)_3]$Δ-$[Os(bpy)_3]$}$(PF_6)_4$ exhibits an interesting behavior under application of magnetic fields. In particular, at low temperature and zero magnetic field, the emission is exclusively vibronically induced due to Herzberg-Teller coupling, since the transition at the lowest electronic origin is symmetry forbidden. By application of a high magnetic field, the electronic 0–0 transition and Franck–Condon activity is effectively tuned in. Thus, the emission spectrum is completely altered. A corresponding property has not yet been reported for other compounds.

In conclusion, the new structure type, as it is realized in {Λ-$[Ru(bpy)_3]$Δ-$[Os(bpy)_3]$}$(PF_6)_4$, is crucially responsible for the occurrence of characteristic photophysical properties. It is indicated that this specific compound represents the first example of a new class of materials.

Acknowledgements

We would like to thank Priv.-Doz. Dr. Josef Breu for many stimulating discussions with respect to crystallographic questions and developments. Financial support by the Stiftung Volkswagenwerk is acknowledged. We also thank the Degussa AG for a donation of $RuCl_3 \cdot 3H_2O$ and $OsCl_3$.

References

[1] B. O'Regan, M. Grätzel, Nature 353 (1991) 737.
[2] A. Hagfeldt, M. Grätzel, Acc. Chem. Res. 33 (2000) 269.
[3] D. Kuciauskas, M.S. Freund, H.B. Gray, J.R. Winkler, N.S. Lewis, J. Phys. Chem. B 105 (2001) 392.
[4] U. Kosch, I. Klimant, T. Werner, O.S. Wolfbeis, Anal. Chem. 70 (1998) 3892.
[5] H. Yersin, W. Humbs, J. Strasser, Top. Curr. Chem. 191 (1997) 153.
[6] H. Yersin, D. Braun, E. Gallhuber, G. Hensler, Ber. Bunsenges. Phys. Chem. 91 (1987) 1228.
[7] H. Yersin, G. Hensler, E. Gallhuber, J. Luminesc. 40-41 (1988) 676.
[8] H. Yersin, D. Braun, G. Hensler, E. Gallhuber, in: C.D. Flint (Ed.), Vibronic Processes in Inorganic Chemistry, Academic Publishers, Kluwer Dordrecht, 1989, p. 195.
[9] M. Furue, S. Konoshita, T. Kushida, Chem. Lett. (Chem. Soc. Japn.) (1987) 2355.

[10] M. Furue, K. Maruyama, Y. Kanematsu, T. Kushida, M. Kamachi, Coord. Chem. Rev. 132 (1994) 201.
[11] V. Balzani, F. Barigelletti, P. Belser, S. Bernhard, L. DeCola, L. Flamigni, J. Phys. Chem. 100 (1996) 16786.
[12] B. Schlicke, P. Belser, L. DeCola, E. Sabbioni, V. Balzani, J. Am. Chem. Soc. 121 (1999) 4207.
[13] A. Harriman, F.M. Romero, R. Ziessel, A.C. Benniston, J. Phys. Chem. A 103 (1999) 5399.
[14] A. Juris, L. Prodi, A. Harriman, R. Ziessel, M. Hissler, A. El-Ghayoury, F. Wu, E.C. Riesgo, R.P. Thummel, Inorg. Chem. 39 (2000) 3590.
[15] L. DeCola, F. Barigelletti, V. Balzani, R. Hage, J.G. Haasnoot, J. Reedijk, J.G. Vos, Chem. Phys. Lett. 178 (1991) 491.
[16] F. Barigelletti, L. Flamigni, J.-P. Collin, J.-P. Sauvage, Chem. Commun. (1997) 333.
[17] M.D. Ward, F. Barigelletti, Coord. Chem. Rev. 216-217 (2001) 127.
[18] M. Devenney, L.A. Worl, S. Gould, A. Guadalupe, B.P. Sullivan, J.V. Caspar, R.L. Leasure, J.R. Gardner, T.J. Meyer, J. Phys. Chem. A 101 (1997) 4535.
[19] G. Giuffrida, G. Calogero, V. Ricevuto, S. Campagna, Inorg. Chem. 34 (1995) 1957.
[20] M. Beley, S. Chodorowki, J.-P. Collin, J.-P. Sauvage, L. Flamigni, F. Barigelletti, Inorg. Chem. 33 (1994) 2543.
[21] K. Shinozaki, Y. Hotta, T. Otsuka, Y. Kaizu, Chem. Lett. (1999) 101.
[22] M. Tsushima, N. Ikeda, A. Yoshimura, K. Nozaki, T. Ohno, Coord. Chem. Rev. 208 (2000) 299.
[23] M. Tsushima, N. Ikeda, K. Nozaki, T. Ohno, J. Phys. Chem. 104 (2000) 5176.
[24] M.E. von Arx, E. Burattini, A. Hauser, L. van Pieterson, R. Pellaux, S. Decurtins, J. Phys. Chem. A 104 (2000) 883.
[25] K. Okamoto, M. Taniguchi, M. Takahashi, A. Yamagishi, Langmuir 17 (2001) 195.
[26] J. Breu, C. Kratzer, H. Yersin, J. Am. Chem. Soc. 122 (2000) 2548.
[27] C. Kratzer, J. Breu, H. Yersin, Proceedings of the 13th International Symposium on Photochemistry and Photophysics of Coordination Compounds, Lipari, Italy, 1999, p. 255.
[28] D.P. Rillema, D.S. Jones, H.A. Levy, J. Chem. Soc. Chem. Commun. (1979) 849.
[29] M. Biner, H.-B. Bürgi, A. Ludi, C. Röhr, J. Am. Chem. Soc. 114 (1992) 5197.
[30] E.C. Constable, P.R. Raithby, D.N. Smit, Polyhedron 8 (1989) 367.
[31] M.M. Richter, B. Scott, K.J. Brewer, R.D. Willett, Acta Crystallogr. C 47 (1991) 2443.
[32] H. Yersin, W. Humbs, J. Strasser, Coord. Chem. Rev. 159 (1997) 325.
[33] H. Yersin, P. Huber, H. Wiedenhofer, Coord. Chem. Rev. 132 (1994) 35.
[34] H. Yersin, E. Gallhuber, A. Vogler, H. Kunkely, J. Am. Chem. Soc. 105 (1983) 4155.
[35] T. Schönherr, J. Degen, E. Gallhuber, G. Hensler, H. Yersin, Chem. Phys. Lett. 158 (1989) 519.
[36] G.A. Crosby, Acc. Chem. Res. 8 (1975) 231.
[37] E.M. Kober, T.J. Meyer, Inorg. Chem. 21 (1982) 3967.
[38] E.M. Kober, T.J. Meyer, Inorg. Chem. 23 (1984) 3877.
[39] A.J. Thomson, V. Skarda, M.J. Cook, D.J. Robbins, J. Chem. Soc. Dalton Trans. (1985) 1781.
[40] H. Yersin, E. Gallhuber, G. Hensler, Chem. Phys. Lett. 134 (1987) 497.
[41] E. Krausz, J. Ferguson, Progress Inorg. Chem. 37 (1989) 293.
[42] (a) D. Braun, E. Gallhuber, H. Yersin, Chem. Phys. Lett. 171 (1990) 122;
(b) D. Braun, E. Gallhuber, H. Yersin, Chem. Phys. Lett. 173 (1990) 132.
[43] C. Daul, E.J. Baerends, P. Vernooijs, Inorg. Chem. 33 (1994) 3538.
[44] Y. Komada, S. Yamauchi, N. Hirota, J. Phys. Chem. 92 (1988) 6511.
[45] M. Kato, S. Yamauchi, N. Hirota, Chem. Phys. Lett. 157 (1989) 543.
[46] H. Yersin, G. Hensler, E. Gallhuber, W. Rettig, L.O. Schwan, Inorg. Chim. Acta 105 (1985) 201.
[47] H. Yersin, D. Braun, Coord. Chem. Rev. 111 (1991) 39.
[48] D. Braun, P. Huber, J. Wudy, J. Schmidt, H. Yersin, J. Phys. Chem. 98 (1994) 8044.
[49] H. Yersin, W. Humbs, Inorg. Chem. 38 (1999) 5820.
[50] A. Yeh, C.V. Shank, J.K. McCusker, Science 289 (2000) 935.
[51] J.K. McCusker, personal communication, Veszprém Hungary, 2001.
[52] H. Yersin, E. Gallhuber, J. Am. Chem. Soc. 106 (1984) 6582.
[53] H. Yersin, E. Gallhuber, G. Hensler, Journal de Physique, Colloque C 7 Suppl. 10 43 (1985) C 7-453.
[54] R.W. Harrigan, G.D. Hager, G.A. Crosby, Chem. Phys. Lett. 21 (1973) 487.
[55] R.W. Harrigan, G.A. Crosby, J. Chem. Phys. 59 (1973) 3468.
[56] G.D. Hager, G.A. Crosby, J. Am. Chem. Soc. 97 (1975) 7031.
[57] G.D. Hager, R.J. Watts, G.A. Crosby, J. Am. Chem. Soc. 97 (1975) 7037.
[58] W.H. Elfring, G.A. Crosby, J. Am. Chem. Soc. 103 (1981) 2683.
[59] H. Yersin, D. Braun, Chem. Phys. Lett. 179 (1991) 85.
[60] B. Henderdon, G.F. Imbusch, Optical Spectroscopy of Inorganic Solids, Clarendon Press, Oxford, 1989.
[61] P.L. Scott, C.D. Jeffries, Phys. Rev. 127 (1962) 32.
[62] A. Abragam, B. Bleaney, Electron Paramagnetic Resonance of Transition Ions, Clarendon Press, Oxford, 1970.
[63] H. Yersin, J. Strasser, Coord. Chem. Rev. 208 (2000) 331.
[64] T. Azumi, M.C. O'Donell, S.P. McGlynn, J. Chem. Phys. 45 (1966) 2735.
[65] D. Braun, H. Yersin, Inorg. Chem. 34 (1995) 1967.
[66] D. Braun, E. Gallhuber, G. Hensler, H. Yersin, Mol. Phys. 67 (1989) 417.
[67] D.L. Dexter, J. Chem. Phys. 21 (1953) 836.
[68] (a) T. Förster, Fluoreszenz Organischer Verbindungen, Vandenhoeck und Ruprecht, Göttingen, 1951;
(b) T. Förster, Ann. Physik 2 (1948) 55.
[69] N.J. Turro, Modern Molecular Photochemistry, Benjamin/Cummings Publishers, Menlo Park, USA, 1978.
[70] H. Riesen, Y. Gao, E. Krausz, Chem. Phys. Lett. 228 (1994) 610.
[71] H. Riesen, L. Wallace, E. Krausz, Inorg. Chem. 39 (2000) 5044.
[72] W. Humbs, H. Yersin, Inorg. Chem. 35 (1996) 2220.
[73] (a) B.J. Pankuch, D.E. Lacky, G.A. Crosby, J. Phys. Chem. 84 (1980) 2061;
(b) D.E. Lacky, B.J. Pankuch, G.A. Crosby, J. Phys. Chem. 84 (1980) 2068.
[74] F. Felix, J. Ferguson, H.U. Güdel, A. Ludi, Chem. Phys. Lett. 62 (1979) 153.
[75] S. Decurtins, F. Felix, J. Ferguson, H.U. Güdel, A. Ludi, J. Am. Chem. Soc. 102 (1980) 4102.
[76] J. Ferguson, F. Herren, Chem. Phys. 76 (1983) 45.
[77] J. Ferguson, F. Herren, E. Krausz, M. Maeder, J. Vrbancich, Coord. Chem. Rev. 64 (1985) 21.
[78] E.M. Kober, B.P. Sullivan, T.J. Meyer, Inorg. Chem. 23 (1984) 2098.
[79] E.M. Kober, J.V. Caspar, R.S. Lumpkin, T.J. Meyer, J. Phys. Chem. 90 (1986) 3722.
[80] T.J. Meyer, Pure Appl. Chem. 58 (1986) 1193.
[81] H. Yersin, E. Gallhuber, G. Hensler, Chem. Phys. Lett. 140 (1987) 157.
[82] H. Yersin, P. Huber, D. Braun, J. Phys. Chem. 94 (1990) 3560.
[83] D. Braun, G. Hensler, E. Gallhuber, H. Yersin, J. Phys. Chem. 95 (1991) 1067.

[84] P. Huber, H. Yersin, J. Phys. Chem. 97 (1993) 12705.
[85] K. Kalyanasundaram, Photochemistry of Polypyridine and Porphyrin Complexes, Academic Press, London, 1992, p. 164.
[86] H. Riesen, E. Krausz, Comments Inorg. Chem. 18 (1995) 27.
[87] The data given are determined for doping of rac-$[Os(bpy)_3]^{2+}$ into rac-$[Ru(bpy)_3](PF_6)_2$ [88].
[88] M. Otte, Diplomarbeit, Universität Regensburg, 1992.
[89] W. Holzapfel, H. Yersin, G. Gliemann, J. Chem. Phys. 74 (1981) 2124.
[90] M. Köhler, D. Schmid, H.C. Wolf, J. Luminesc. 14 (1976) 41.
[91] C. Kratzer, Diplomarbeit, Universität Regensburg, 1999.
[92] H. Yersin, D. Donges, Top. Curr. Chem. 214 (2001) 81.
[93] D. Trümbach, Ph.D. Thesis, Universität Regensburg, 1995.
[94] H. Yersin, D. Trümbach, H. Wiedenhofer, Inorg. Chem. 38 (1999) 1411.
[95] J.M. Harrowfield, A.N. Sobolev, Aust. J. Chem. 47 (1994) 763.
[96] E. Krausz, H. Riesen, A.D. Rae, Aust. J. Chem. 48 (1995) 929.
[97] A.C. Albrecht, J. Chem. Phys. 38 (1963) 354.
[98] G. Fischer, Vibronic Coupling, Academic Press, London (GB), 1984.
[99] C.D. Flint (Ed.),Vibronic Processes in Inorganic Chemistry NATO ASI Series C, vol. 288, Kluwer Academic Publishers, Dordrecht, 1989.
[100] N. Mataga, T. Kubota, Molecular Interactions and Electronic Spectra, Marcel Dekker, New York, 1970.
[101] In Refs. [5,65,66,83], state **II** of site A of $[Os(bpy)_3]^{2+}$ doped into rac-$[Ru(bpy)_3](PF_6)_2$ was designated as **Γ** due to its small spectroscopic importance, while state **III**(A) of the present paper corresponds to state **II**(A) in the earlier studies.
[102] J. Wudy, unpublished results (1993).
[103] E. Gallhuber, Ph.D. Thesis, Universität Regensburg, 1989.
[104] E. Gallhuber, G. Hensler, H. Yersin, J. Am. Chem. Soc. 109 (1987) 4818.
[105] G. Gliemann, Comments Inorg. Chem. 5 (1987) 263.
[106] G. Gliemann, Proceedings of the 31st International Congress of Pure and Applied Chemistry, Sofia, Bulgaria, Pergamon, Oxford England Inorganic Chemistry, 1987, p. 11.
[107] G. Gliemann, H. Yersin, Structure and Bonding (Springer Berlin) 62 (1985) 87.
[108] H. Yersin, C. Kratzer, Chem. Phys. Lett. Submitted.
[109] C.J. Ballhausen, Molecular Electronic Structures of Transition Metal Complexes, McGraw Hill, New York, 1979.
[110] E.I. Solomon, Comments Inorg. Chem. 3 (1984) 225.
[111] T.C. Brunhold, H.U. Güdel, In: E.I. Solomon, A.B.P. Lever (Eds.), Inorganic Electronic Structure and Spectroscopy, vol. 1, Wiley, p. 259.